EFFECT OF STRONTIUM ON CALCITE GROWTH RATES UNDER VARYING CALCIUM-TO-CARBONATE RATIOS

A Thesis
Presented to
The Academic Faculty

By

Jacquelyn Nicole Bracco

In Partial Fulfillment
Of the Requirements for the Degree
Master of Science in Earth and Atmospheric Sciences

Georgia Institute of Technology

May 2012

EFFECT OF STRONTIUM ON CALCITE GROWTH RATES UNDER VARYING CALCIUM-TO-CARBONATE RATIOS

Approved by:

Dr. Ellery Ingall, Advisor
School of Earth and Atmospheric Sciences
Georgia Institute of Technology

Dr. Lawrence Bottomley
School of Chemistry and Biochemistry
Georgia Institute of Technology

Dr. Andrew G. Stack
Chemical Sciences Division
Oak Ridge National Laboratory

Date Approved: 19 March 2012

ACKNOWLEDGEMENTS

I would like to thank my advisors, Dr. Andrew Stack and Dr. Ellery Ingall, for the opportunity to work on this project and their patience and scientific guidance. I would also like to thank Dr. Lawrence Bottomley for serving on my committee and for providing insight on how to solve some of the challenges encountered with the experimental setup. A special thanks goes to Meg Grantham for the endless amount of help she provided when equipment would break and for help in interpreting results and her instruction on experiment design/implementation. I would also like to thank the former members of the Stack lab group, Morgan Warren, Dr. Mengni Zhang, Dr. Xuefeng Wang, and Cindy Jackson for encouragement and support. I am grateful to Dr. Dave Wesolowski and the Geochemistry and Interfacial Sciences Group at Oak Ridge National Laboratory for providing funding for this project as well as scientific guidance and assistance. Finally, I would like to thank my friends and family for their encouragement and patience.

Research sponsored by the Division of Chemical Sciences, Geosciences, and Biosciences, Office of Basic Energy Sciences, U.S. Department of Energy.

TABLE OF CONTENTS

LIST OF TABLES

LIST OF FIGURES

LIST OF SYMBOLS

a	Width of a single molecular row of a calcite step (0.31 nm)
A	Scan size (nm/scan)
C_B	Concentration of growth units in the bulk
C_B^{eq}	Equilibrium solubility
Ca_{aq}	Aqueous calcium ion
Ca_{kink}	Calcium adsorbed to a step
$[Ca]/[CO_3]$	Aqueous calcium to carbonate ratio
$[Ca]_s$	Predicted concentration of calcium adsorbed to a step
$CO_{3\ aq}$	Aqueous carbonate ion
$CO_{3\ kink}$	Carbonate adsorbed to a step
D_s	Surface diffusion coefficient
ε/kT	Energy barrier for formation of a kink
h	Height of the step
L	Terrace width between steps
k_{BS}	First order rate constant for attachment of growth units to the surface
k_{Ca}	Rate constant for attachment of calcium
k_{-Ca}	Rate constant for detachment of calcium
k_{CO_3}	Rate constant for attachment of carbonate
k_{-CO_3}	Rate constant for detachment of carbonate
K_{ex}	Cation exchange constant for exchange of a strontium ion adsorbed to a step and a calcium ion adsorbed to a step

k_{SB}	First order rate constant for detachment of growth units from the surface
K_{sp}	Solubility Product
$K_{S\text{-}Ca}$	Equilibrium constant for formation of a calcium precursor site
$K_{S\text{-}Sr}$	$_E$quilibrium constant for formation of a strontium precursor site
N_L	Sampling rate (lines/scan)
r	Ionic ratio (Zhang and Nancollas, 1998)
R_{BCF}	Growth rate of a crystal predicted by BCF theory
r_c	Critical radius
R_{kn}	Rate of kink site nucleation
R_{kp}	Rate of kink site propagation
$k_{\text{-}kn}$	Pseudo-zeroth order detachment rate constant
R_s	Scan rate (lines/s)
S	Saturation ratio (Zhang and Nancollas, 1998)
SI	Saturation Index
$[\text{Sr}]/[\text{Ca}]_{v_{1/2}}$	Strontium-to-calcium ratio at which $v = v_{max}/2$
$step_{total}$	Total number of adsorption sites on the calcite steps
[*step-Ca*]	Aqueous calcium ion adsorbed to a site on a step
[*step-Sr*]	Aqueous strontium ion adsorbed to a site on a step
[Sr]/[Ca]	Aqueous strontium to calcium ratio
V	Molar volume
v_{max}	Maximum step velocity
v_{step}	Step velocity of a single monomolecular step

χ^2	Chi-squared (statistical analysis)
x_s	Characteristic diffusion distance

SUMMARY

Growth and dissolution of the mineral calcite is important for prediction and control of surface and subsurface water quality, calculation of past sea-surface temperatures using paleoenvironmental proxies, and sequestration of contaminants through engineered calcite precipitation. At high concentrations of strontium, calcite growth is known to be inhibited, but the mechanism by which strontium inhibits growth is not well understood. Seeking to better understand this mechanism, atomic force microscopy is used with a flow-through fluid cell to measure real time growth rates of the obtuse and acute monomolecular step orientations on the $\{10\bar{1}4\}$ calcite surface. Growth was measured at two saturation indices as a function of the ratio of the concentrations of aqueous calcium-to-carbonate and varying aqueous strontium concentration. It was found that the amount of strontium required to inhibit growth correlated with the aqueous calcium concentration, but did not correlate with carbonate concentration. This suggests that strontium inhibits attachment of calcium, but not carbonate, during growth. Analytical models of nucleation and propagation of steps are expanded from previous studies to capture multiple saturation indices.

CHAPTER 1: INTRODUCTION

1.1 Motivation

The kinetics of growth of the ubiquitous mineral calcite is of particular interest to geochemists because calcite is the most stable form of calcium carbonate at conditions found on and near the Earth's surface. As such, many rocks contain appreciable amounts of calcite and other calcium carbonate minerals. These rocks affect the composition of ground and surface waters. During both abiotic and biogenic crystallization of calcite, trace metals, such as strontium and magnesium, are incorporated into crystal lattices. The extent to which these ions incorporate has important implications for natural and engineered processes and has been shown to be affected by precipitation rates, temperature, and water chemistry (Lorens, 1981; Tesoriero and Pankow, 1996; Tang et al., 2008; Gebrehiwet et al., 2012; Lea et al., 1999; Russell et al., 2004). For example, the effect of temperature on incorporation enables researchers to measure strontium-to-calcium ratios in biogenic calcite and aragonite. Researchers then utilize these ratios to extrapolate sea surface temperatures (SST) from the recent past and many thousands of years ago. Additionally, strontium is of particular interest because radioactive strontium produced during nuclear weapons testing is present at contaminated DOE sites and exceeds DOE guidelines. Strontium concentrations range from 0.05 to 231,000 pCi/L in groundwater and 0.02 to 540,000 pCi/L in soils and sediments, but DOE guidelines require strontium levels not exceed 1000 pCi/L (Riley, 1992). Immobilization of strontium by co-precipitating it into calcite is a potential method for removing this radioactive strontium from the subsurface. Since calcite is a sparingly soluble mineral,

this enables long term sequestering of strontium necessary for radioactive strontium to decay (Gebrehiwet, et al., 2012).

At high concentrations, strontium inhibits calcite growth by a process that is not well understood. The goals of this thesis are to determine the mechanism by which strontium affects growth and to determine if current crystal growth models can explain inhibition of growth by strontium. In this thesis, atomic force microscopy (AFM) was used to measure the growth rates of monomolecular steps on calcite surfaces in real-time and to observe the evolution of the morphology of the calcite surface.

The format of this thesis is as follows. Chapter 1 comprises a discussion of historical and current crystal growth theories, including Kossel crystal growth theory, BCF (Burton, Cabrera, and Frank) crystal growth theory, an electrolyte crystal growth model proposed by Zhang and Nancollas (the kinetic ionic ratio model), and a recent crystal growth model specifically designed for calcite proposed by Stack and Grantham (referred to as a kink site nucleation model). Chapter 1 also includes detailed information on carbonate mineralogy. Further details about engineered remediation of strontium and the use of strontium-to-calcium ratios in biogenic calcite to calculate sea surface temperatures are also presented.

Chapter 2 provides information on the methods used in this study, including how growth rates were calculated from AFM images. Growth was measured at two saturation indices as a function of the ratio of the concentrations of aqueous calcium-to-carbonate and under varying aqueous strontium concentration, and the specific solution compositions are included in the chapter. Chapter 2 also includes details on parameterization of the experiments, such as how experimental conditions were chosen to

ensure mass transport of calcium and carbonate ions were not limiting growth rates and to ensure the growth rates measured were at steady state.

Chapter 3 presents the results of this study. The concentration of strontium necessary to inhibit growth was found to be correlated with the concentration of calcium in solution, but was not found to be correlated with the concentration of carbonate in solution. Our original hypothesis was that strontium inhibits calcite growth by preventing carbonate ions from attaching to the calcite surface. Since there is no correlation between carbonate and strontium but there is between strontium and calcium, strontium must be affecting attachment of calcium. Two of the theories discussed in chapter 1 (the kinetic ionic ratio model and the kink site nucleation model) were tested to determine if either could predict experimentally calculated step velocities in the absence of strontium. Step velocities predicted for solution compositions not containing strontium with the kinetic ionic ratio model were much more inaccurate than those predicted using the kink site nucleation model. The kink site nucleation model was also adapted to account for the effect of strontium. Finally, chapter 4 includes the conclusions and suggestions for future work.

1.2 Crystal Growth Theory

Atomic force microscopy has allowed an unprecedented ability to examine the structure of mineral surfaces and study many surface processes, including adsorption, crystal growth and dissolution. In particular, *in situ* crystal growth and dissolution experiments have enabled researchers to test historical and modern crystal growth theories to examine the reactions governing these processes. On the surface of minerals, flat regions, called terraces, can be observed using AFM. If the crystal surface is not

perfectly flat, steps, which may be straight or rough, can also be observed separating these terraces. These steps also contain sites called kink sites that are thought to be more reactive than other sites on the surface (shown diagrammatically in Figure 1.1). If the steps are rough, there are large amounts of kink sites present, whereas if they are smooth, the kink site density is smaller.

The basic building blocks of the crystal (which may be ions or molecules) are thought to preferentially attach to kink sites because there the ion or molecule will be able to form multiple bonds to the surface. Attachment to flat terraces will be the least favorable because the ions or molecules can make fewer the bonds to the surface there. As such, the ion or molecule is more likely to detach since the rate of detachment is proportional to the inverse of the number of bonds to the surface. Under supersaturated solutions (where crystal growth normally occurs), the attachment rate is greater than the detachment rate because the solution contains a higher concentration of these building blocks than what the bulk solubility dictates. During growth, advancement of monomolecular steps across the crystal surface can be observed using AFM. In this thesis, crystal growth theories are discussed in terms of growth for conciseness, however these models also can be applied to crystal dissolution, as the underlying theory is similar. With regards to dissolution, there is a net rate of detachment of ions or molecules from the surface and ions or molecules will most readily detach from terraces and least readily from kink sites. This leads to retreat of steps across a crystal, rather than the advancement observed during crystal growth.

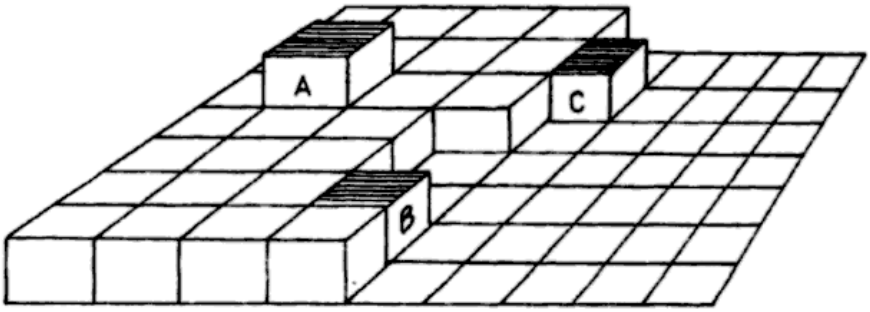

Figure 2.1 A diagram of representative sites on a surface based on the terrace-step-kink model. A is a growth unit adsorbed to a terrace, B is a growth unit adsorbed to a kink site, and C is a growth unit adsorbed to a step. From Crystal Growth: Principles and Progress (Vere, 1987).

Kossel Crystal Growth Theory

Kossel and Stranski (Kossel, 1927; Stranski, 1928) published the first work to recognize that defects on crystal surfaces are often the controlling factor in the rate of nucleation of kink sites. These defects may arise from various factors such as lattice mismatch and incorporation of impurities into crystals. Their theory, also referred to as the terrace-step-kink model, treats crystals as a simple cubic lattice with a single type of building block for growth, referred to as a growth unit. Based on this theory, the growth unit for a calcite crystal is a $CaCO_3$ formula unit; thus, this theory does not encompass independent attachment and detachment of calcium and carbonate ions. This constrains growth to a maximum at stoichiometric ratios of aqueous calcium to carbonate. However, researchers have determined that growth may be maximized at ratios higher than unity (Stack and Grantham, 2010; Tai et al., 2005; Gebrehiwet et al., 2012). This implies that the concept of a formula unit as the basic building block is an oversimplification because the ions attach independently. To form a step on a flat

terrace, a growth unit would need to adsorb to the crystal surface, which requires high supersaturation (50% or greater) to be favorable. However, this conflicts with later experimental studies measuring crystal growth at low supersaturation (Burton et al., 1951). This is because even at low supersaturation (1% and lower), crystals will have steps and kink sites arising from thermal fluctuations (Frenkel, 1945; Burton et al., 1951).

BCF Crystal Growth Theory

Kossel crystal growth theory provided the framework for Burton, Cabrera, and Frank (1951) to develop their seminal crystal growth theory. BCF theory, which is also based on a simple cubic lattice with a single type of growth unit, introduces surface dislocations referred to as screw dislocations. These dislocations provide a constant source of steps to which growth units can attach, commonly referred to as a growth hillock (Figure 1.2), which eliminates the need for high supersaturation required for Kossel crystal growth. Despite this, the supersaturation of the solution is still a key factor in predicting advancement speeds of steps, the more supersaturated a solution is, the greater the rate of attachment of growth units to the surface. BCF suggested dislocations arise from shear stress in the crystal, but during experimental observations using AFM, it appears many of these growth hillocks actually form on grain boundaries.

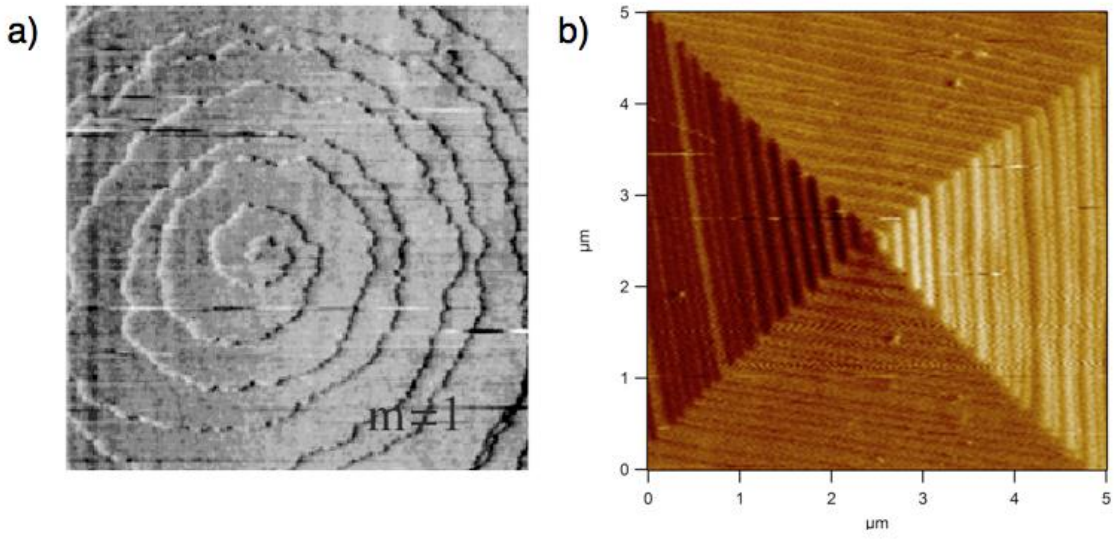

Figure 1.2 AFM deflection images of spiral growth hillocks on a) the {100} potassium dihydrogen phosphate (KDP) surface (from Thomas et al., 2003) and b) the $\{10\bar{1}4\}$ calcite surface. The rough steps on KDP indicate kink site density is high and the growth rate is limited by kink site propagation rather than the nucleation of kinks. The straight steps on calcite indicate kink site nucleation is controlling growth and kink site propagation is rapid.

BCF theory postulated that mineral growth close to equilibrium could be thought of as being limited by either transport of ions to the parent phase or surface processes, such as adsorption of growth units to the surface and diffusion of growth units on the surface to kink sites (Burton et al., 1951). For minerals with low solubility, surface processes are generally thought to limit growth more than transport, while minerals with a high solubility are thought to be limited more by transport of ions from the bulk to the surface (Berner, 1978; Lasaga, 1998), though in reality a mix of both processes is actually controlling growth. In order to isolate the kinetics of surface reactions, crystal growth experiments of low-solubility minerals, such as calcite and barite, are normally designed to have a constant flux of growth units to the surface so that mass transport is

not limiting growth (Teng et al., 2000). This enables researchers to determine what the rate limiting reactions are for mineral growth and dissolution.

In this model, growth rate can be described as a function of the velocity of the steps advancing across the surface, v_{step}, and the distance between the steps, L. The distance between steps can range from small, indicating steps are generated rapidly from a highly supersaturated solution, to large, such as for slow growth from a near-equilibrium solution. During the time it takes a step to advance this distance, the maximum height of the surface has increased by the height of the step, h. The rate is described as:

$$R_{BCF} = \frac{v_{step} h}{L} \tag{1.1}$$

Finally, this theory predicts the diffusion rate of these loosely bound growth units to kink sites along the surface will also affect step advancement. By including diffusion, step velocities can be described as:

$$v_{step} = 2D_s \frac{\bar{V}}{h} \frac{k_{BS}}{k_{SB}} \frac{(C_B - C_B^{eq})}{x_s} \tanh\left(\frac{L}{2x_s}\right) \tag{1.2}$$

where D_s is the surface diffusion coefficient, V is the molar volume, k_{BS} and k_{SB} are the first order rate constants for attachment and detachment of growth units to and from the surface respectively, C_B is the concentration of growth units in the bulk, C_B^{eq} is the equilibrium solubility, x_s is the characteristic diffusion distance, and L is the distance between steps. This in turn can be solved geometrically from the distance between the arms of an ideal spiral:

$$L \approx 19 r_c \tag{1.3}$$

where r_c is the critical radius, the radius of two-dimensional nuclei on the surface where either growth or decay of the nuclei will reduce the free energy of the system (i.e., the Gibbs free energy is maximized, also referred to as the Gibbs-Thomson effect; De Yoreo et al., 2003; De Yoreo et al., 2009). As supersaturation increases, the critical radius decreases linearly and the Gibbs free energy increases proportionally. By combining equations 1.1-1.3, an overall equation for the rate of growth can be expressed as:

$$R_{BCF} = 2D_s \frac{\bar{V}}{h} \frac{k_{BS}}{k_{SB}} \frac{(C_B - C_B^{eq})}{x_s} \tanh\left(\frac{19r_c}{2x_s}\right) \frac{h}{19r_c} \tag{1.4}$$

Since the critical radius depends on supersaturation, at low supersaturation the growth rate will depend quadratically on the saturation state, but at high supersaturation the growth rate will depend linearly on the saturation state. Two key assumptions of this theory are that kink site generation is high regardless of the saturation state and the proportion of ions (for crystals comprised of more than one type of ion) in solution is assumed to be stoichiometric. Additionally surface diffusion does not control crystal growth of calcite (Gratz et al., 1993), leading to the possibility that this model may not be able to accurately predict step velocities on calcite.

At equilibrium, kink sites will be randomly generated through thermal fluctuations (i.e. attachment, detachment, and diffusion of growth units along a surface) at the step edge (Frenkel, 1945). Overall the rates of attachment and detachment of growth units will be equal, leading to no net growth or dissolution. Moving from equilibrium to supersaturated conditions, natural fluctuations at the step edge need to be compared to the fluctuations arising from perturbation away from equilibrium by determining if kink site nucleation is fast enough to maintain a high density of kink sites. If the two types of fluctuations cannot be distinguished, the fluctuation dissipation

theorem of non-equilibrium thermodynamics (Chandler, 1987) applies and BCF theory can be used to predict the rate of crystal growth. This is the case for many high solubility minerals that have a low energy barrier for formation of a kink (ε/kT is much less than unity), such as KDP (De Yoreo et al., 2009; Figure 1.2a). However, if the two types of fluctuations can be distinguished from one another, this indicates the fluctuation dissipation theorem does not apply. As a result, the Gibbs-Thomson effect no longer applies because there is a large energy barrier for kink formation (ε/kT is greater than unity) and the rate of kink formation does not minimize the Gibbs free energy (suggesting the critical radius no longer scales with supersaturation). For these minerals, BCF theory cannot describe the rate of crystal growth.

Using atomic force microscopy (AFM), it can be determined if the fluctuation dissipation theorem is likely to apply by examining the shape of steps and growth hillocks. If the steps are rough and growth hillocks are somewhat circular in shape, many kink sites are present and the fluctuation dissipation theorem may apply (Figure 1.2a). If the steps are smooth (Figure 1.2b) and growth hillocks are polygonized, the rate at which growth units attach to preexisting kink sites (kink site propagation) is much more rapid than the formation of new kink sites, thus kink site nucleation is controlling growth and the fluctuation dissipation theorem likely does not apply. In the case of calcite and other sparingly soluble minerals, kink site propagation is fast, leading to low kink site densities as a result of weak step fluctuations (De Yoreo et al., 2009). As a result, to model growth of sparing soluble minerals, the rate of growth predicted by the model must be limited by kink site nucleation.

Modern Crystal Growth Theory (Zhang and Nancollas's Kinetic Ionic Ratio Model)

Due to the inherent limitations of BCF theory, Zhang and Nancollas (1998) developed the kinetic ionic ratio model to describe growth and dissolution of sparingly soluble ionic minerals, in particular minerals comprised of two constituent ions. In the case of calcite, the two constituent ions are calcium and carbonate. Step advancement is predicted as a function of the saturation ratio:

$$S = \left[\frac{\{\mathrm{Ca}\}\{\mathrm{CO_3}\}}{K_{sp}} \right]^{1/2} \tag{1.5}$$

where {Ca} and {CO_3} are the activities of calcium and carbonate in solution and K_{sp} is the equilibrium solubility product ($10^{-8.48}$; Plummer and Busenberg, 1982). To account for decreased growth at ratios far from unity, a correction factor is included which is based on the ionic ratio:

$$r = \frac{k_{Ca}\{\mathrm{Ca}\}}{k_{CO_3}\{\mathrm{CO_3}\}} \tag{1.6}$$

where k_{Ca} and k_{CO_3} are the attachment rate constants for calcium and carbonate. This theory was derived using the structure of the {001} face of a crystal with a NaCl (halite) type lattice, which has an isometric structure where each cation and anion in the lattice is surrounded by six nearest neighbors in an octahedral coordination. While this is likely the simplest structure for an AB ionic crystal, halite is not a sparingly soluble mineral and dissolution of halite occurs five orders of magnitude faster than dissolution of calcite and barite ($BaSO_4$) (Berner, 1978). Calcite has a rhombohedral structure and barite has an orthorhombic structure, which lead to different bonding environments for ions and molecules in the crystal lattice than for halite: cations in calcite are coordinated by six oxygen ions each belonging to a different carbonate and cations in barite are coordinated

by twelve oxygen ions belonging to seven different sulfates. This likely affects the applicability of this theory to either of these minerals.

Zhang and Nancollas derived elementary rate constants for their model by making four different assumptions, which included: (a) the deposition rate of each ion is proportional to its activity in solution and does not depend on the site on a step to which the ion attaches, (b) the detachment frequency is proportional to the binding energy of ions to a given site (as discussed above detachment will occur more frequently from terraces than kink sites due to fewer bonds to the surface), (c) the detachment frequencies are the same for both ions (it is assumed that the same bond is broken for each type of ion, then $\varepsilon_A = \varepsilon_B = \varepsilon$), and (d) detachment from a non-kink site (under supersaturated conditions) and attachment of ions to a non-kink site (under undersaturated conditions) can be neglected. Assumption (c) is of particular concern because detachment rates calculated using molecular dynamics have not been shown to be equal for barium and sulfate ions detaching from a barite step (Stack, 2009). Calcium and carbonate ions detaching from calcite will also likely have different detachment energies as detachment from the surface will be affected by complexation or protonation of ions and detachment of carbonate may be related to the solubility product.

The 1D nucleation rate can be defined as:

$$R_{kn} = K_{sp}^{0.5}\left[\frac{k_{Ca}\{\mathrm{Ca}\}}{k_{Ca}\{\mathrm{Ca}\}+k_{-Ca}}+\frac{k_{CO_3}\{CO_3\}}{k_{CO_3}\{CO_3\}+k_{-CO_3}}\right]\exp(-2\varepsilon/\mathrm{kT})\left(\frac{\{\mathrm{Ca}\}\{\mathrm{CO_3}\}}{K_{sp}}-1\right)(k_{Ca}k_{CO_3})^{0.5} \quad (1.7)$$

and the rate of kink site propagation can be written as:

$$R_{kn} = K_{sp}^{0.5}\left[\frac{k_{Ca}\{\mathrm{Ca}\}}{k_{Ca}\{\mathrm{Ca}\}+k_{-Ca}}+\frac{k_{CO_3}\{\mathrm{CO_3}\}}{k_{CO_3}\{\mathrm{CO_3}\}+k_{-CO_3}}\right]\exp(-2\varepsilon/\mathrm{kT})\left(\frac{\{\mathrm{Ca}\}\{\mathrm{CO_3}\}}{K_{sp}}-1\right)(k_{Ca}k_{CO_3})^{0.5} \quad (1.8)$$

where k_{-Ca} and k_{-CO_3} are the rate constants for detachment of calcium and carbonate and ε/kT is the energy barrier for kink formation. The rate at which steps advance depends on the density of kink sites (which is dependent on both kink site nucleation and kink site propagation), the kink site propagation rate, and the spacing between ions A and B in the lattice. Step velocity can be predicted by including correction functions for the effect of the nonstoichiometric ratios and rewriting the equations as a function of the saturation ratio and ionic ratio:

$$v_{step} = 2a(S^{2.5} - S^{0.5})\left[\frac{1}{S(r^{0.5} + r^{-0.5}) + 2}\left(\frac{1}{S + r^{0.5}} + \frac{1}{S + r^{-0.5}}\right)\right]^{1/2} \exp(-\varepsilon/\mathrm{kT}) K_{sp}^{0.5} (k_{Ca} k_{CO_3})^{0.5} \quad (1.9)$$

This theory predicts low step velocities for ratios far from unity, which have been experimentally observed by multiple researchers (Stack and Grantham, 2010; Gebrehiwet et al., 2012; Perdikouri et al., 2009; Larsen et al., 2010). However, the model fails to reproduce zero or negative step velocities experimentally measured under supersaturated conditions for low solubility minerals such as calcite (Stack and Grantham, 2010; Fan et al., 2006). This is because the predicted detachment frequency from a kink is a function of the solubility of the mineral and the square root of the attachment rate constants multiplied together. Since calcite has a very low solubility ($10^{-8.48}$), attachment is predicted to be higher than detachment even at very high or low ratios. One other problem with this theory is that since equation 1.9 is a function of kink site nucleation and kink site propagation, the rate of kink site nucleation cannot be rate limiting, which has been found to be the case for calcite (De Yoreo et al., 2009).

Kink-Site Nucleation Limited Theory

To develop a model that can predict zero or negative step velocities, Stack and Grantham (2010) adapted modern crystal growth theory to enable attachment and detachment rates to be independent of each other, while still allowing constituent ions to be treated as separate growth units. The following reactions govern kink site formation in this model:

$$\mathrm{Ca}^{2+}_{aq} \underset{k_{-Ca}}{\overset{k_{Ca}}{\rightleftharpoons}} \mathrm{Ca}_{\mathrm{kink}} \tag{1.10}$$

$$\mathrm{CO}^{2-}_{3\ aq} \underset{k_{-CO_3}}{\overset{k_{CO_3}}{\rightleftharpoons}} \mathrm{CO}_{3\ \mathrm{kink}} \tag{1.11}$$

where k_{Ca} and k_{CO_3} are the rate constant for attachment of aqueous calcium and carbonate ions to a step, k_{-Ca} and k_{-CO_3} are the rate constants for detachment of adsorbed calcium and carbonate ions from a kink site, $\mathrm{Ca_{aq}}$ and $\mathrm{CO_{3\ aq}}$ are the aqueous calcium and carbonate ions and $\mathrm{Ca_{kink}}$ and $\mathrm{CO_{3\ kink}}$ are the ions adsorbed to the step.

Since calcite is a sparingly soluble mineral, the rate of kink site nucleation can be assumed to be limiting growth and the rate of kink site propagation is fast. This gives us a velocity dependent solely on the rate of kink site nucleation:

$$v_{step} = aR_{kn} \tag{1.12}$$

where a is the width of a single molecular row of a calcite step (0.31 nm) and the rate of kink site nucleation is defined as:

$$R_{kn} = \frac{k_{Ca}[\mathrm{Ca}]k_{CO_3}[\mathrm{CO_3}]}{k_{Ca}[\mathrm{Ca}] + k_{CO_3}[\mathrm{CO_3}]} - k_{-kn} \tag{1.13}$$

The rate constants are the same as those defined in (1.10) and (1.11), [Ca] and [CO_3] are the concentrations of calcium and carbonate in solution, and k_{-kn} is a pseudo-zeroth order

rate constant that includes the overall rate of detachment and the density of kink sites. The propagation reaction may need to be considered in some cases, such as where attachment or detachment of either calcium or carbonate is rate limiting, which may occur at very high or low calcium-to-carbonate ratios. At these ratios, steps begin to roughen and curve, indicating the propagation of kinks is occurring at a slower rate than at ratios close to unity (Stack and Grantham, 2010). Growth in the presence of impurities has also been found to cause steps to roughen and curve (Figure 1.3). The same propagation rate defined by Zhang and Nancollas (1998) can be used here:

$$R_{kp} = \frac{k_{Ca}[\mathrm{Ca}]k_{CO_3}[\mathrm{CO_3}] - k_{-kpCa}k_{-kpCO_3}}{k_{Ca}[\mathrm{Ca}] + k_{CO_3}[\mathrm{CO_3}] - k_{-kpCa} - k_{-kpCO_3}} \tag{1.14}$$

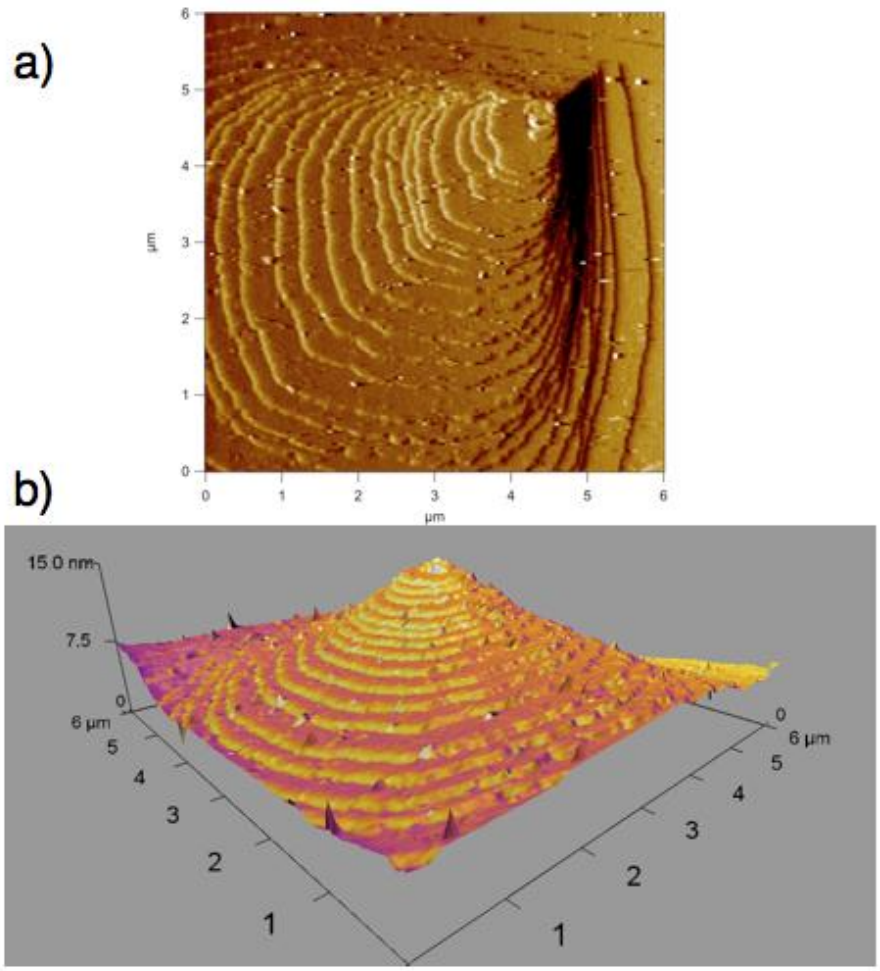

Figure 1.3 AFM deflection images of spiral growth hillocks on the {10-14} calcite surface in the presence of strontium. Image b) is a three-dimensional representation of a) where the height image is colored with the deflection data. The image is exaggerated 400 fold in the z direction. The rough steps on calcite in the presence of strontium indicate kink site propagation is likely less rapid than in the absence of strontium and the growth rate is limited by nucleation and propagation.

While this theory represents an advance over preexisting theories, future work focusing on accounting for the effects of background electrolytes, pH effects, and better constraining the detachment reactions by determining the density of kink sites would increase the applicability of this model. Additionally, a recent computational study using rare event theory to probe kink site formation on barite, a sparingly soluble mineral with

two constituent ions, indicates barium ions detach from the surface by proceeding from a bound state (a kink site) to a species with two bonds to the surface to an inner-sphere adsorbed species to an outer-sphere adsorbed species before diffusing into solution (Stack et al., 2012). The rate-limiting step for detachment of the barium ion to form a kink is moving from an inner-sphere to an outer-sphere species, while the rate-limiting step for attachment is the transition from an inner-sphere species to a species with two bonds to the surface. It is possible that similar reactions also take place on calcite, and if so the attachment and detachment rate constants in equations 1.10 and 1.11 are strictly constants for the overall reaction described by the model.

1.3 Carbonate mineralogy

Major rock-forming anhydrous carbonate minerals are classified into one of three structurally unique groups, the calcite group, the aragonite group, and the dolomite group. Generally, cations with an ionic radius smaller than calcium form carbonates of the calcite-like structure and cations with an ionic radius larger than calcium, such as strontium, form carbonates of the aragonite-like structure. The calcite group structure is traditionally derived from the cubic structure of NaCl (described above in the Zhang and Nancollas theory section) by replacing sodium with calcium (or another divalent metal such as magnesium) and chloride with carbonate. Since carbonate ions are trigonal planar but chloride ions are spherical, the crystal lattice shifts to a rhombohedral structure with a three-fold rotoinversion axis of symmetry and a glide plane along the *c*-crystallographic axis (the space group is $R\bar{3}c$; Figure 1.4). Metal cations (such as calcium) are coordinated by six oxygen ions, each from a different carbonate, while oxygen ions are coordinated by two metal ions and a carbon. The metal oxygen bond is a

weaker bond than the C-O bond, thus calcite cleaves along the $\{10\bar{1}4\}$ plane, which minimizes the number of Ca-O bonds broken and does not break any C-O bonds (Reeder, 1983). The surface created by this cleavage is the one most commonly studied during *in situ* AFM experiments. Larger divalent metals, such as strontium and barium, are not usually accommodated in a stable 6-coordination in large quantities and are instead coordinated by nine of the oxygen ions, which results in an orthorhombic crystal structure where oxygen ions are coordinated by a carbon and three metal ions (i.e., the aragonite lattice) (Speer, 1983).

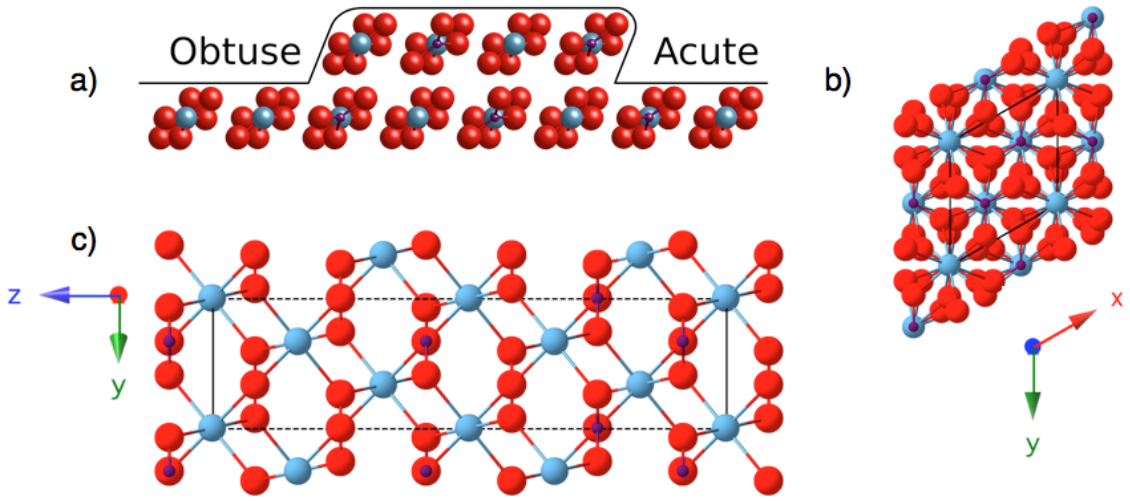

Figure 1.4 a) A cross-sectional representation of the two distinct step orientations, obtuse and acute, on the $\{10\bar{1}4\}$ calcite surface and the calcite unit cell as viewed along b) the a axis and c) the c axis.

1.4 Elemental Paleoproxies

As calcium carbonate minerals grow, divalent metals, such as strontium, can incorporate into the crystal lattice. Large divalent cations, such as strontium, substitute at much higher concentrations into aragonite than calcite (de Villiers et al., 1994; Cohen and McConnaughey, 2003), while small cations substitute more prevalently into calcite and affect growth at the calcite surface differently than large cations (Wasylenki et al., 2005a). Strontium-to-calcium ratios in biogenic calcite and aragonite are a popular elemental proxy for paleoclimatologists to use in reconstructing past sea surface temperature (SST). While strontium is found in much lower concentrations in seawater than calcium and magnesium, it is still one of the most abundant calcium-substituting cations in natural environments (Pingitore et al., 1992). Strontium-to-calcium ratios in biogenic calcium carbonates appear to correlate with temperature and water chemistry, among other environmental parameters (Lea et al., 1999; Russell et al., 2004). As a result, modern corals are often used to quantify climate variability due to natural and anthropogenic effects during the past century, as well as quantify El Niño Southern Oscillation (ENSO) variability (Cohen and McConnaughey, 2003). Older corals from thousands of years ago enable reconstruction of paleoenvironments at a resolution higher than that of other paleoproxies, such as $\delta^{18}O$. These corals are only analyzed for years to decades worth of continuous time because of limits on how long corals grow, so conditions affecting the Sr/Ca ratio, such as pH and salinity, often are assumed to be constant (Cohen and McConnaughey, 2003). If aragonite in corals is replaced with strontium-depleted calcite through diagenesis, significantly different temperatures may be predicted however (Sayani et al., 2011).

While many studies have measured the effects of various chemical and physical environmental factors, there is disagreement over which factors exert the most influence over strontium partitioning and incorporation rates. A model was recently developed by DePaolo (2011) to predict metal/calcium ratios in calcite as a function of precipitation rate. They established that the strontium-to-calcium ratio in the mineral is a result of the competition between precipitation and exchanges between the fluid and calcite. Researchers also recently discovered foraminifera incorporate higher concentrations of strontium when the aqueous calcium concentration is increased at constant supersaturation (increasing the calcium-to-carbonate ratio), but incorporation is not increased when the aqueous carbonate concentration is increased (decreasing the calcium-to-carbonate ratio) at constant supersaturation (Duenas-Bohorquez et al., 2011; Raitzsch et al., 2010). It is unclear if this is a vital effect or if these phenomena might be affected by factors also affecting abiotic calcite growth, suggesting further research to constrain the effect on strontium on abiotic calcite growth is necessary.

1.5 Remediation of strontium

Engineered precipitation of minerals that can incorporate impurities has been suggested as a method to remediate subsurface contamination, such as to immobilize radioactive strontium via incorporation into calcite (Tartakovsky et al., 2008). The effect of strontium on calcite growth has been examined through bulk precipitation experiments, which have shown that strontium incorporation into calcite increases as precipitation rate increases (Lorens, 1981; Tesoriero and Pankow, 1996; Tang et al., 2008; Gebrehiwet et al., 2012). Using an electron microprobe, Wasylenki and coworkers (2005a) also observed higher incorporation of strontium at higher precipitation rates and

preferential incorporation into the obtuse (as opposed to acute) step orientation on $\{10\bar{1}4\}$ surfaces. Using atomic force microscopy (AFM), they observed morphological changes and determined strontium has complex effects on calcite growth rate. Strontium modestly enhances calcite growth rates at low strontium concentrations, but a critical concentration is reached that causes growth rates to collapse as the aqueous strontium concentration is increased.

During engineered precipitation, concentration gradients form because the porous media in the subsurface are poorly-mixed environments. This can lead to regions where the calcium concentration is much higher than the carbonate concentration and vice versus. To determine the effect of these gradients on strontium incorporation, a recent bulk precipitation experiment studied incorporation into calcite and found the distribution coefficient for strontium into calcite is not affected by the calcium-to-carbonate ratio at concentrations of strontium less than those required to inhibit growth (Gebrehiwet et al., 2012). Additionally, it has been shown the cation-to-anion ratio asymmetrically affects the rate of growth for minerals such as calcite (Stack and Grantham, 2010; Perdikouri et al., 2009; Larsen et al., 2010) and barite (Kowacz et al., 2007). Stack and Grantham (2010) also found that the peak step velocity for the two orientations occurs at different calcium-to-carbonate ratios, acute steps advanced fastest under low calcium-to-carbonate ratios whereas the obtuse steps advanced fastest under higher calcium-to-carbonate ratios.

Here using AFM with a flow-through fluid cell using establish methods (Land et al., 1997; Teng et al., 2000), we examine the effect of strontium on calcite growth as a function of this aqueous calcium-to-carbonate ratio to determine if it impacts the effect of strontium on calcite growth. We measured these growth rates under varying ratio at a

variety of concentrations of strontium ranging up to the concentration required to inhibit growth. We conclude that the concentration of strontium required to inhibit growth correlates with the aqueous concentration of calcium ion, but is not correlated with either the strontium-to-carbonate ratio or the product of strontium and carbonate, indicating strontium is likely affecting attachment of calcium to the calcite surface.

CHAPTER 2: METHODS

2.1 Sample and Growth Solution Preparation

Stock solutions used to prepare growth solutions were created from ACS reagent grade $CaCl_2$, $NaHCO_3$, and $SrCl_2$ dissolved in distilled, deionized water (18.2 MΩ-cm) and equilibrated with the atmosphere for at least two weeks or sparged with air overnight prior to use. We found that use of solutions not equilibrated with the atmosphere resulted in increased acute step velocities at low calcium-to-carbonate ratios, likely due to incomplete equilibration with carbon dioxide (Figure 2.1).

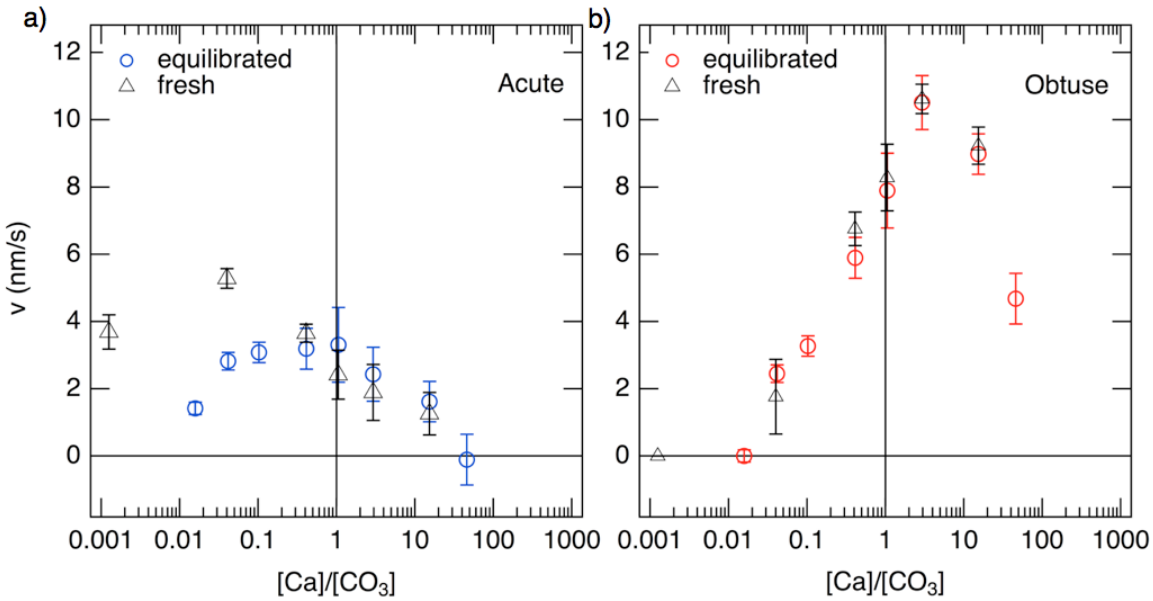

Figure 2.1 Growth of the a) acute and b) obtuse calcite steps as a function of the aqueous calcium-to-carbonate ratio at a fixed saturation index of 0.40. Red and blue circles denote the orientations exposed to solutions equilibrated with atmospheric CO_2 (from Stack and Grantham, 2010), while the black triangles denote the steps exposed to solutions not equilibrated with atmospheric CO_2. Equilibration does not appear to affect measured growth rates for the obtuse orientation, but measured velocities are higher for the acute orientation at low calcium-to-carbonate ratios.

The chemical compositions of the growth solutions were calculated using PHREEQC (Parkhurst, 1995), treating the system as equilibrated with the atmosphere. The pH of inlet and outlet solutions were measured to confirm that the pH of the growth solution matched the pH calculated using PHREEQC to a few tenths of a pH unit. Depending on the solution composition, pH varied from 8.5 (at high calcium-to-carbonate ratios) to 9.2 (at low calcium-to-carbonate ratios). Saturation indices were kept fixed at SI = 0.40 and SI = 0.75 ($SI = \log(Ca \times CO_3 / K_{sp})$). Saturation indices greater than zero correspond to supersaturation and saturation indices less than zero correspond to undersaturation. The aqueous calcium-to-carbonate ratio was varied from 0.0143 to 381 for SI = 0.75 and 0.0158 to 45.8 for SI = 0.40. Strontium concentrations in each of the solutions used were in the range of 0 to 9.07×10^{-3} M. The specific solution compositions used can be found in Table 2.1 for the solutions without added strontium and Table 2.2a-b for the solutions with added strontium. No additional background electrolyte was added to the growth solutions since the amount and identify of background electrolytes has been shown to affect growth rates (Ruiz-Agudo et al., 2011). Here, the ionic strength of the growth solutions were all less than 0.02.

Table 2.1: Solution composition summary for SI = 0.75 without added strontium. Columns are $[Ca^{2+}]/[CO_3^{2-}]$ ratio, concentration of reactants ($[Ca^{2+}]$, $[CO_3^{2-}]$), activities of reactants (aCa^{2+}, aCO_3^{2-}), and calculated and measured pH.

$[Ca^{2+}]/[CO_3^{2}]$	$[Ca^{2+}]$ (moles/l)	$[CO_3^{2-}]$ (moles/l)	$a\ Ca^{2+}$	$a\ CO_3^{2-}$	calculated pH	measured pH
0.0143	2.76e-5	1.94e-3	1.62e-5	1.14e-3	9.35	9.09 (±0.23)
0.0312	3.81e-5	1.22e-3	2.37e-5	7.59e-4	9.27	9.08 (±0.26)
0.111	6.68e-5	6.02e-4	4.48e-5	4.04e-4	9.13	9.09 (±0.096)
1.27	2.13e-4	1.68e-4	1.57e-4	1.23e-4	8.87	9.07 (±0.17)
4.88	4.11e-4	8.42e-5	3.10e-4	6.34e-5	8.73	9.00 (±0.23)
27.2	9.63e-4	3.55e-5	7.16e-4	2.64e-5	8.54	8.68 (±0.25)
43.2	1.22e-3	2.81e-5	8.92e-4	2.07e-5	8.48	8.73 (±0.18)
381	4.23e-3	1.11e-5	2.68e-3	7.02e-6	8.25	8.41 (±0.070)

Table 2.2a: Solution composition summary for SI =0.75 with added strontium. Columns are $[Ca^{2+}]/[CO_3^{2-}]$ ratio, concentration of reactants ($[Ca^{2+}]$, $[Sr^{2+}]$, $[CO_3^{2-}]$), and activities of reactants (aCa^{2+}, aSr^{2+}, aCO_3^{2-}).

$[Ca^{2+}]/[CO_3^{2-}]$	$[Sr^{2+}]/[Ca^{2+}]$	$[Ca^{2+}]$ (moles/l)	$[CO_3^{2-}]$ (moles/l)	$[Sr^{2+}]$ (moles/l)	$a\ Ca^{2+}$	$a\ CO_3^{2-}$	$a\ Sr^{2+}$
27.2	0.0102	9.64e-4	3.55e-5	9.84e-6	7.15e-4	2.63e-5	7.32e-6
	0.0358	9.64e-4	3.55e-5	3.45e-5	7.15e-4	2.63e-5	2.56e-5
	0.0766	9.64e-4	3.55e-5	7.38e-5	7.13e-4	2.62e-5	5.46e-5
	0.102	9.64e-4	3.55e-5	9.84e-5	7.11e-3	2.62e-5	7.27e-5
	0.153	9.64e-4	3.55e-5	1.48e-4	7.09e-3	2.61e-5	1.09e-4
	0.408	9.66e-4	3.55e-5	3.94e-4	6.97e-4	2.56e-5	2.85e-4
	0.612	9.67e-4	3.55e-5	5.92e-4	6.89e-4	2.53e-5	4.22e-4
	1.02	9.73e-4	3.58e-5	9.92e-4	6.76e-4	2.49e-5	6.90e-4
	1.52	9.70e-4	3.54e-5	1.48e-3	6.56e-4	2.39e-5	1.00e-3
0.0143	0.313	2.77e-5	1.94e-3	8.65e-6	1.62e-5	1.14e-3	5.09e-6
	0.722	2.77e-5	1.93e-3	2.00e-5	1.62e-5	1.13e-3	1.18e-5
	1.08	2.77e-5	1.93e-3	3.00e-5	1.62e-5	1.13e-3	1.76e-5
	1.44	2.77e-5	1.93e-3	4.00e-5	1.62e-5	1.13e-3	2.35e-5
	1.80	2.77e-5	1.93e-3	5.00e-5	1.63e-5	1.13e-3	2.94e-5
	2.16	2.78e-5	1.93e-3	6.00e-5	1.63e-5	1.13e-3	3.53e-5
381	0.119	4.24e-3	1.11e-5	5.05e-4	2.63e-3	6.89e-6	3.13e-4
	0.237	4.24e-3	1.11e-5	1.01e-3	2.58e-3	6.77e-6	6.13e-4
	0.355	4.24e-3	1.11e-5	1.51e-3	2.54e-3	6.66e-6	9.04e-4
	0.474	4.24e-3	1.11e-5	2.01e-3	2.50e-3	6.55e-6	1.19e-3
	0.592	4.24e-3	1.11e-5	2.51e-3	2.46e-3	6.45e-6	1.46e-3
	0.889	4.25e-3	1.11e-5	3.77e-3	2.37e-3	6.21e-6	2.12e-3
	1.00	4.23e-3	1.10e-5	4.26e-3	2.33e-3	6.08e-6	2.36e-3
	1.13	4.25e-3	1.11e-5	4.78e-3	2.31e-3	6.05e-6	2.61e-3
	1.36	4.25e-3	1.11e-5	5.79e-3	2.26e-3	5.89e-6	3.09e-3
	1.84	4.25e-3	1.10e-5	7.81e-3	2.17e-3	5.62e-6	4.00e-3
	2.13	4.26e-3	1.10e-5	9.07e-3	2.12e-3	5.47e-6	4.53e-3

Table 2.2b: Solution composition summary for SI = 0.40 with added strontium.
Columns are same as in Table 2.2a.

$[Ca^{2+}]/[CO_3^{2-}]$	$[Sr^{2+}]/[Ca^{2+}]$	$[Ca^{2+}]$ (moles/l)	$[CO_3^{2-}]$ (moles/l)	$[Sr^{2+}]$ (moles/l)	$a\ Ca^{2+}$	$a\ CO_3^{2-}$	$a\ Sr^{2+}$
2.72	0.364	1.98e-4	7.19e-5	7.21e-5	1.52e-4	5.53e-5	5.54e-5
	0.606	1.98e-4	7.18e-5	1.20e-4	1.52e-4	5.50e-5	9.20e-5
	0.848	1.98e-4	7.17e-5	1.68e-4	1.51e-4	5.47e-5	1.28e-4
	1.04	1.98e-4	7.16e-5	2.07e-4	1.51e-4	5.44e-5	1.57e-4
	1.21	1.98e-4	7.15e-5	2.40e-4	1.50e-4	5.42e-5	1.82e-4
	1.45	1.98e-4	7.14e-5	2.88e-4	1.50e-4	5.39e-5	2.18e-4
	1.69	1.99e-4	7.13e-5	3.36e-4	1.49e-4	5.36e-5	2.53e-4
0.111	0.391	4.29e-5	4.35e-4	1.68e-5	2.97e-5	3.01e-4	1.16e-5
	0.684	4.30e-5	4.35e-4	2.94e-5	2.97e-5	3.01e-4	2.04e-5
	0.977	4.30e-5	4.34e-4	4.20e-5	2.97e-5	3.00e-4	2.91e-5
	1.27	4.30e-5	4.34e-4	5.46e-5	2.97e-5	3.00e-4	3.78e-5
12.1	0.235	4.17e-4	3.45e-5	9.80e-5	3.23e-4	2.67e-5	7.59e-5
	0.470	4.17e-4	3.44e-5	1.96e-4	3.20e-4	2.64e-5	1.50e-4
	0.705	4.17e-4	3.43e-5	2.94e-4	3.17e-4	2.61e-5	2.24e-4
	0.939	4.17e-4	3.43e-5	3.91e-4	3.14e-4	2.59e-5	2.95e-4
	1.17	4.17e-4	3.42e-5	4.89e-4	3.12e-4	2.56e-5	3.66e-4
	1.41	4.16e-4	3.41e-5	5.86e-4	3.09e-4	2.54e-5	4.36e-4

Calcite samples (Wards Scientific) were cleaved along the $\{10\bar{1}4\}$ surface. A representative calcite sample was analyzed using inductively coupled plasma optical emission spectrometry (ICP-OES) to determine trace divalent cations impurity content (Table 2.3). Of the different impurities measured, magnesium was the most common at 588 ppm. While some trace strontium was observed in the calcite samples, the concentrations were negligible compared to the amounts added to the growth solutions.

Table 2.3: Trace divalent metal concentrations in parts per million in a representative calcite sample.

Mg	Sr	Fe	Mn
588	45.5	54.8	65.2

2.2 In situ AFM Experiments

In the experiments shown here, two atomic force microscopes were used to measure step velocities on freshly cleaved calcite samples, an Agilent PicoPlus and an Asylum Research MFP-3D. Prior to mounting samples, calcite dust produced during cleaving was removed using compressed nitrogen. The $\{10\bar{1}4\}$ calcite surface was exposed to growth solutions continuously flowing at a rate of 120 mL/hr with the obtuse step orientation facing the inlet solution, a flow rate and direction under which growth was not limited by mass transport to the surface for fluid cells used with both microscopes. When growth solutions were flowing at a rate of 60 mL/hr, calculated step velocities were less than those measured at flow rates of greater than 90 mL/hr, indicating transport of ions to the surface is affecting growth at lower flow rates and growth is not strictly controlled by processes occurring on the calcite surface (Figure 2.2).

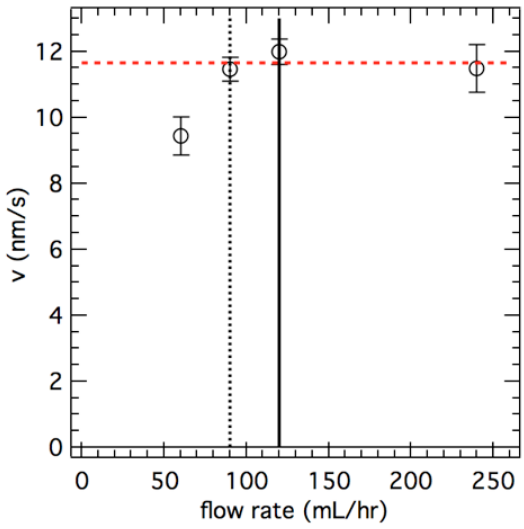

Figure 2.2 Step velocity of the obtuse step orientation as a function of the flow rate of the growth solution. The dotted black line indicates the approximate flow rate required to reach a step velocity not limited by mass transport (denoted by the red dotted line). The bolded line at 120 mL/hr is the flow rate at which the step velocities reported in this thesis were measured, ensuring that the velocities were not affected by mass transport to the surface.

After each new growth solution was introduced to the fluid cell, the system was allowed to relax back to a steady-state step velocity. The time required for this was found to be approximately 26 minutes for the fluid cell used with the Agilent PicoPlus AFM and 19 minutes for the fluid cell used with the Asylum Research MFP-3D AFM (Figure 2.3). To ensure steady state was reached, step velocities were calculated from images collected at least 40 minutes after the initial injection of each solution into the cell. Step velocities for the obtuse and acute steps on the $\{10\bar{1}4\}$ calcite surface were measured on growth features known as spiral growth hillocks.

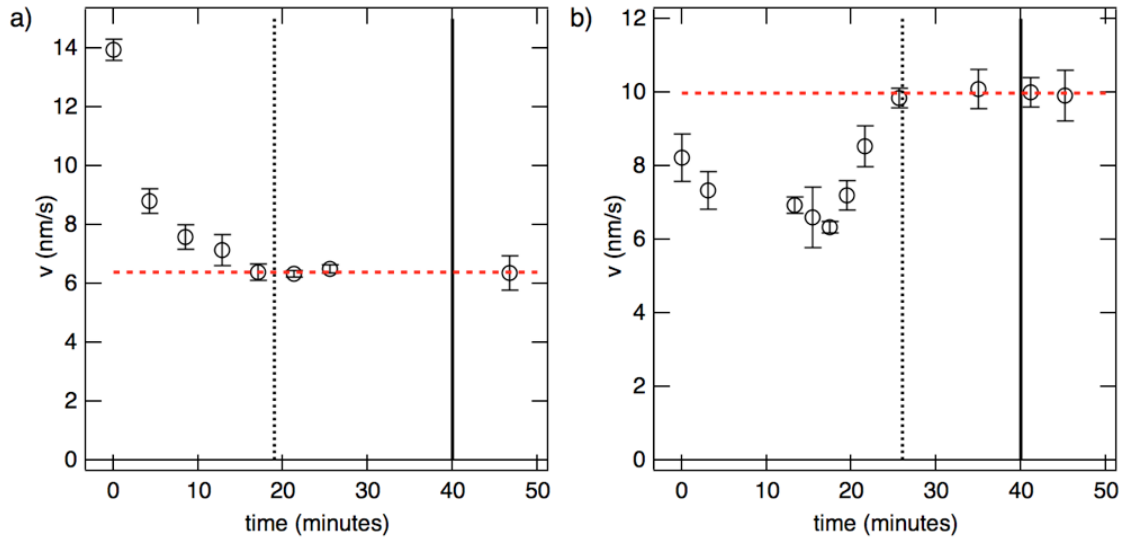

Figure 2.3 Step velocity of the obtuse step orientation as a function of time since introducing a new solution to the fluid cell used with an a) Asylum Research MFP-3D AFM and b) Agilent PicoPlus AFM. The dotted black line indicates the approximate time it takes to reach the steady state step velocity (denoted by the red dotted line). The bolded line at forty minutes is the time at which the step velocities reported in this thesis were measured, ensuring that the velocities were measured at steady state.

2.3 Image Analysis

During imaging, deflection and height images for the trace and retrace of the tip across the surface were collected. Unaltered trace and retrace deflection images were primarily used in image analysis, however height images could also be used if the images were subjected to a first order flatten and a first order planefit along the fast scan direction prior to analysis. During flattening individual least-squares fit polynomials are calculated and then subtracted from each scan line. This corrects bowing and slope of the image in the slow scan direction and differences in scan height from one scan line to another. A planefit corrects the tilt and bowing along the fast scan direction by subtracting a polynomial from the image. No filtering of the images was necessary. In this thesis all AFM images, with the exception of Figure 1.3b, are raw deflection images. Figure 1.3b is a height image that has been colored with the corresponding deflection image. The height image has been subjected to a first order flatten and a first order planefit. After this, a few scan lines were removed using the erase scan line tool found in the Asylum Research software. This tool works by replacing the selected line by interpolation.

Step velocities were primarily measured by calculating the velocity from the slope of the trace of the step over time (Figure 2.4):

$$v_{step} = \frac{R_s A}{N_L tan\theta} \tag{2.1}$$

where R_s is the scan rate (lines/s), A is the scan size (nm/scan), N_L is the sampling rate (lines/scan), and θ is the measured angle.

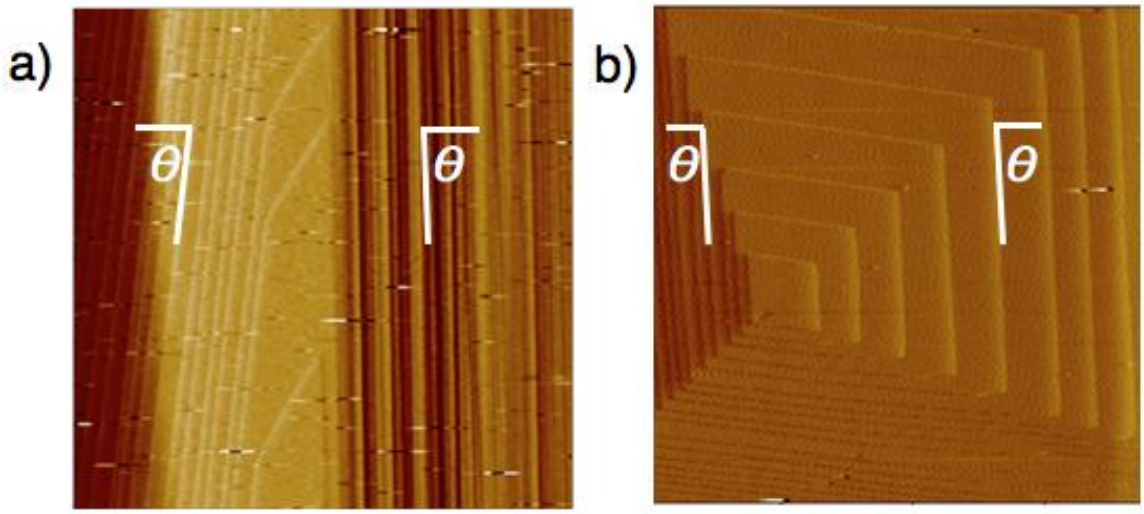

Figure 2.4 Measurements of angles on two different deflection images of calcite growth hillocks with the slow scan axis a) disabled and b) enabled. Both images are from scans where the tip was moving down relative to the top of the image (the scan size for both images is 7.5 μM*)*. The crystal in a) is aligned so the angle measured during an up and a down scan is the same, so the calculated velocity is the actual velocity for both scan directions. The crystal in b) is misaligned, so the measured angle for the acute steps during a down scan is greater than 90 leading to a negative calculated velocity, much less than the actual velocity. During an up scan the angle is less than 90 leading to a calculated positive velocity much greater than the actual velocity, but in this thesis it is shown that the average of the two scans is the same as the actual velocity.

As the curvature and irregularity of the steps increased with increasing strontium concentrations, velocities were measured by calculating the displacement of points on individual steps in sequential images. Generally the tip was rastered at an angle where the velocities measured during up and down scans were similar, but the velocities were corrected for thermal scanner drift or misalignment of the calcite crystal by taking the average of both an up and a down scan. Figure 2.5 presents a proof concluding that if these two scan directions are averaged, then misalignment of the calcite crystal does not impact the calculated step velocities. Two to four replicates were performed per data point (the velocities quoted below are the mean of the replicates and error bars are ± one standard deviation).

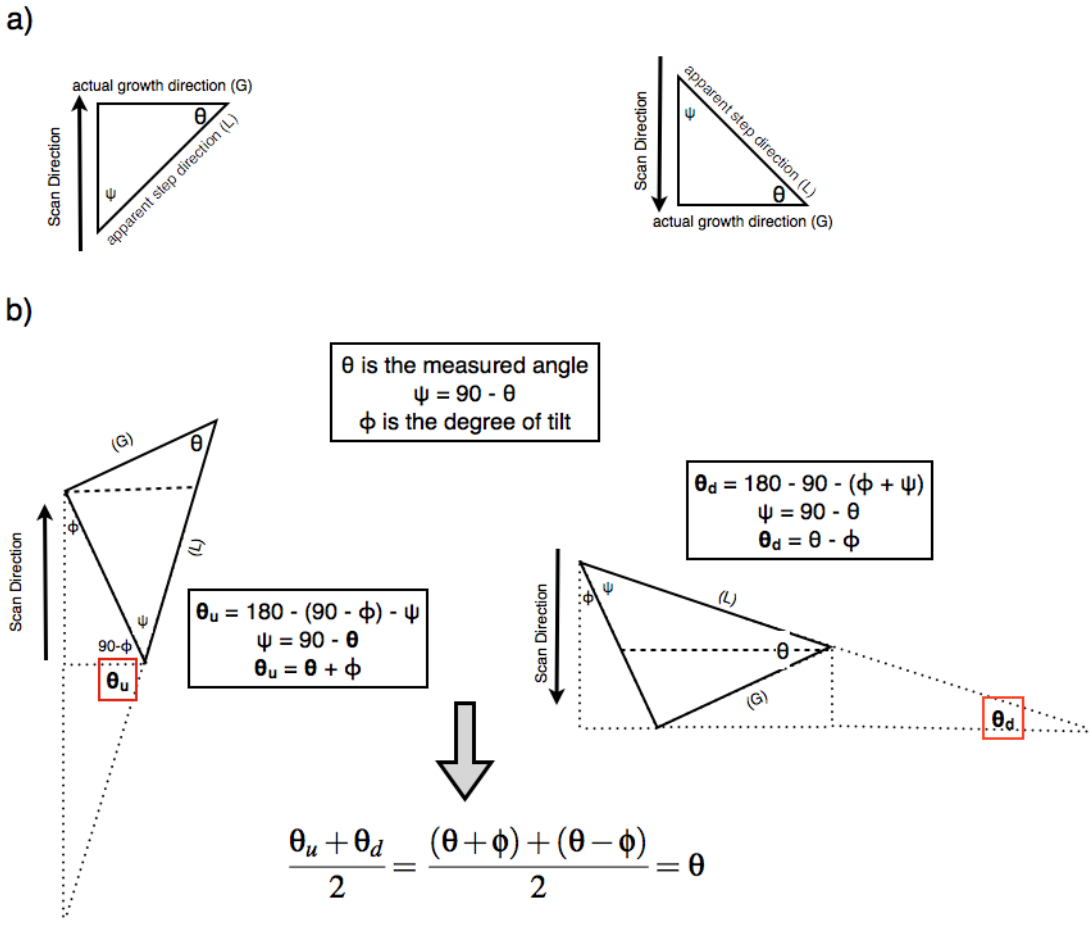

Figure 2.5 Proof that the orientation of the crystal does not affect the step velocities measured if an up and a down scan are averaged where a) is an aligned crystal and b) is a misaligned crystal. The apparent step direction (L) is a convolution of the actual growth direction (G) and the scan direction. θ is the angle measured on the hillock, ϕ is the degree of the tilt of the crystal, and ψ is 90 – θ. If the crystal is misaligned, the measured angle for an up scan will be less than the angle that would be measured for an aligned crystal and vice versus for the down scan. This degree of difference will be the same for both scan directions, so if the angles for both directions are averaged, the misalignment does not affect calculated velocities.

CHAPTER 3: RESULTS AND DISCUSSION

3.1 In-situ AFM observations at SI = 0.40 and 0.75 in the absence of strontium.

Step velocities of the obtuse and acute step orientations on calcite growth hillocks were measured at a fixed saturation index (SI = 0.75), but variable aqueous calcium-to-carbonate ratio (Figure 3.1). The step velocities measured here follow a trend similar to step velocities previously reported by Stack and Grantham (2010) who measured velocities at a lower saturation index (SI = 0.40). That is, the peak velocity of the obtuse steps occurs at high calcium-to-carbonate ratios, whereas the acute steps advance fastest at ratios close to stoichiometric (1:1) or slightly lower. As expected, the magnitude of the step velocities is greater at the larger saturation index used here, particularly for the obtuse step orientation. However, at the saturation index of 0.75, steps were observed to continue to advance under solutions containing aqueous calcium-to-carbonate ratios far from stoichiometric, which is in contrast to the behavior observed at a saturation index of 0.40. Morphology is also similar between the two saturation indices, where obtuse steps became rounded at low ratios and bunching of the acute step occurred at high ratios.

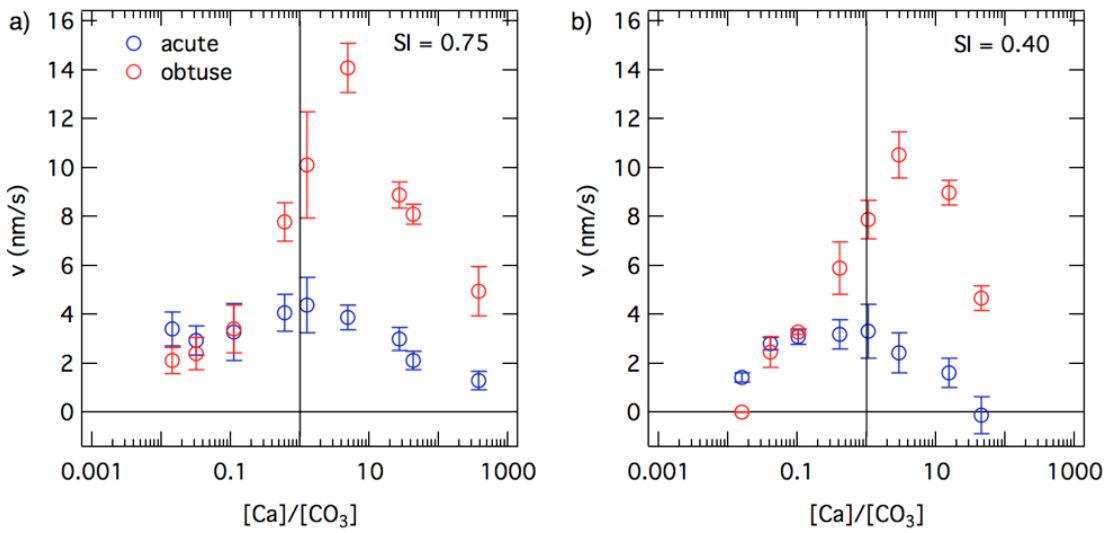

Figure 3.1: Step velocities as a function of calcium-to-carbonate ratios at a saturation index of 0.40 and 0.75. Obtuse steps advance faster at high ratios, whereas the acute step grows more rapidly at ratios close to one, or slightly lower than one. Error bars are ± 1 standard deviation.

As there was approximately twice as much data for SI = 0.75 as SI = 0.40, each data point in the SI = 0.40 data was doubled to give equal weighting of each data set in the fits that are described below. The difference between fit parameters calculated from the doubled SI = 0.40 dataset and the undoubled dataset was determined not to be statistically significant using a heteroscedastic two-tailed *t*-test. The *t*-value can be calculated using the following equation and compared to the *t*-critical value to determine if the means are statically different:

$$t = \frac{\bar{X}_1 - \bar{X}_2}{\sqrt{\frac{s_1^2}{n_1} + \frac{s_2^2}{n_2}}} \tag{3.1}$$

where *t* is the *t*-value, X_1 and X_2 are the means of the two samples, s_1^2 and s_2^2 are the sample variances, and n_1 and n_2 are the sample sizes. The degrees of freedom can be calculated using the following equation:

$$d.f. = \frac{\left(s_1^2/n_1 + s_2^2/n_2\right)^2}{(s_1^2/n_1)^2/(n_1-1) + (s_2^2/n_2)^2/(n_2-1)} \tag{3.2}$$

A heteroscedastic test was chosen because the variances were not found to be statistically equal using an *F*-test. An *F*-test compares the variances of two of the different fit parameters (such as the fit parameter for calcium attaching to an obtuse step and the fit parameter for carbonate attaching to an obtuse step). The more the ratio between the two variances deviates from one, the more likely it is that the samples have unequal variances.

The combined SI = 0.75 and SI = 0.40 dataset was simultaneously fit to the kinetic ionic ratio model (Zhang and Nancollas, 1998) and fit parameters were estimated using a Newton-Raphson minimization. The χ^2 was 1740 for the obtuse orientation and 321 for the acute orientation. The analytical expression used to fit the step velocity data is equation 1.9, found in the introduction. The model fits are shown in Figure 3.2 and the fit parameters are shown in Table 3.1. Importantly, the model can neither predict step velocities of both saturation indices simultaneously (i.e., using the same rate constants for both), nor can it replicate the shapes of the curve well for obtuse step orientation at a saturation index of 0.75.

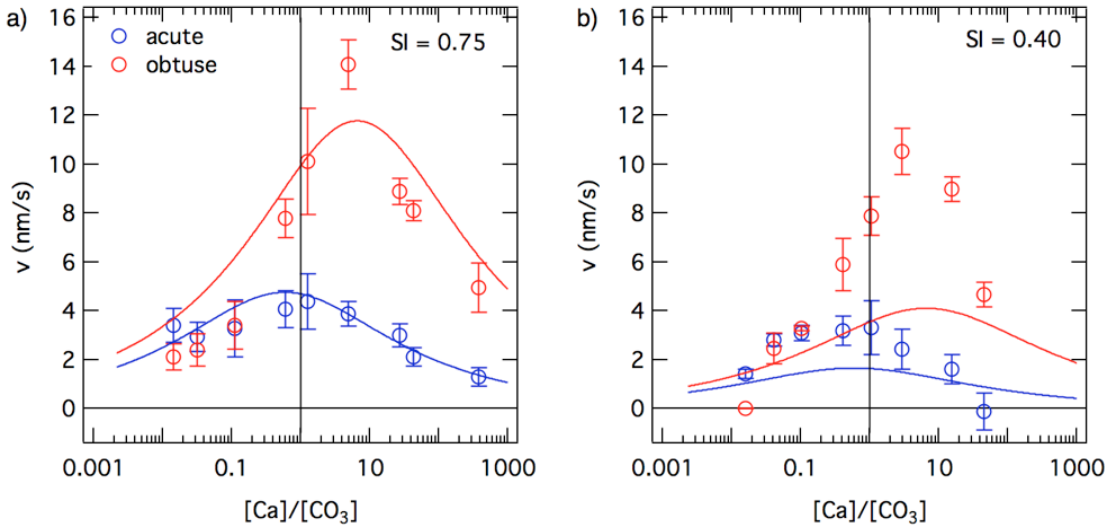

Figure 3.2: Step velocities as a function of calcium-to-carbonate ratios at a saturation index of a) 0.75 and b) 0.40. Curves are model fits of the combined data set (SI = 0.40 and 0.75) using the Zhang and Nancollas (1998) kinetic ionic ratio model. Error bars are ± 1 standard deviation and the chi-squared for the obtuse fit is 1780 and 321 for the acute fit, both of which are much higher than the chi-squared values for the kink site nucleation model (Stack and Grantham, 2010).

Table 3.1: Estimates of rate constants for the Zhang and Nancollas (1998) model.

Constants	**acute** (χ^2 = 321)	**obtuse** (χ^2 = 1740)
k_{Ca} (s^{-1})	1.8×10^8	1.3×10^8
k_{CO_3} (s^{-1})	1.1×10^8	8.7×10^8

Attempting to obtain a model that suitably describes multiple saturation states, we switch to using the kink-nucleation limited model previously derived in Stack and Grantham (2010) and adapted from crystal growth theory (De Yoreo and Vekilov, 2003; De Yoreo et al., 2009). This model does not explicitly include saturation state as a master variable but treats attachments and detachments of calcium and carbonate ions independently based on their respective concentrations. This model is presented in more detail in Section 1.2, in the portion entitled "Kink-Site Nucleation Limited Theory".

Figure 3.3 shows the step velocity model fit to the two saturation indices simultaneously; fit parameters are shown in Table 3.2. The fit is much more suitable for both step orientations and saturation indices than the kinetic ionic ratio model. The χ^2 was 417 for the obtuse orientation and 195 for the acute orientation. These values are much lower than the kinetic ionic ratio model, though the model underestimates step velocities for the acute step orientation at high calcium-to-carbonate ratios for the saturation index of 0.75 and at low calcium-to-carbonate ratios for the saturation index of 0.40. Additionally, the fit also underestimates the peak obtuse step velocity at a saturation index of 0.40 and predicts nonzero step velocities at ratios where step advancement was not observed. The calculated attachment rate for calcium ions is ~2 orders of magnitude smaller than the water exchange rate of the aqueous ion (Richens, 1997) and a computationally estimated rate constant for attachment to planar surfaces (Kerisit, 2004), however this is a reasonable estimate given that attachment and detachment of ions at steps on mineral surfaces may be a multi-step process (Stack et al., 2012).

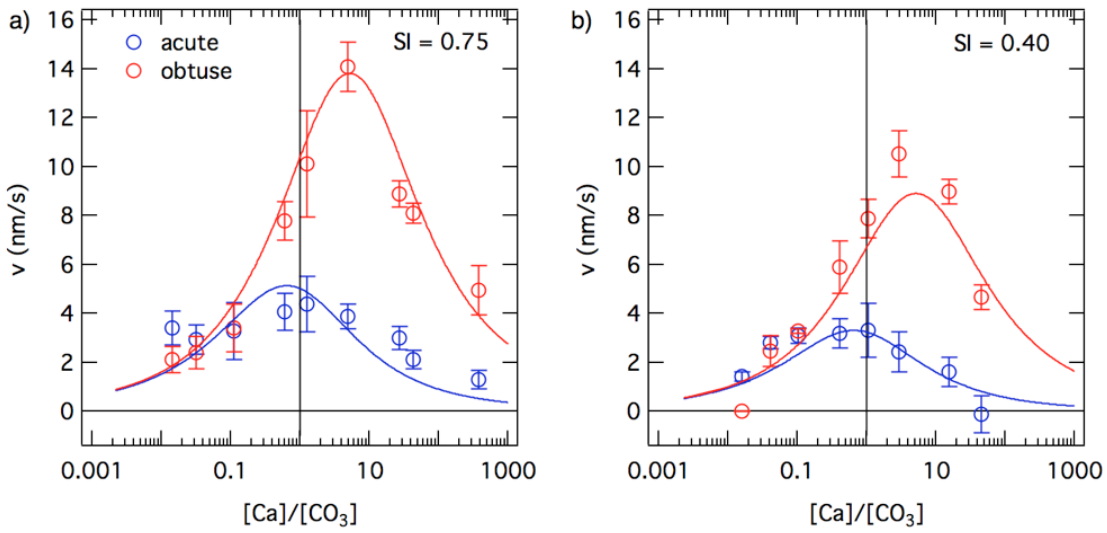

Figure 3.3: Step velocities as a function of calcium-to-carbonate ratios at a saturation index of 0.40 and 0.75. Curves are model fits of the combined data set (SI = 0.40 and 0.75) using the kink site nucleation model from Stack and Grantham (2010). Error bars are ± 1 standard deviation and the χ^2 for the obtuse fit is 418 and 195 for the acute fit.

Table 3.2: Estimates of rate constants for the nucleation model (Stack and Grantham, 2010). Values are the best estimate, standard deviations estimated from residuals are shown in parentheses.

Constants	acute	obtuse
k_{Ca} (s^{-1})	6.4 (± 0.5) × 10^6	6.7 (± 0.3) × 10^6
k_{CO_3} (s^{-1})	4.7 (± 0.4) × 10^6	3.6 (± 0.2) × 10^7
k_{-kn} ($M \cdot s^{-1}$)	0.0 (± 0.02)	0.0 (± 0.02)

The magnitude of the fit parameters is smaller than the fit parameters reported in Stack and Grantham (2010). Forcing the model to zero velocity at the same ratios as reported in Stack and Grantham (2010), yielded fit parameters within error of those parameters reported in Stack and Grantham (2010). However, the resulting χ^2 values were much larger (1030 for the obtuse orientation and 297 for the acute orientation), indicating the fit is likely worse than if the model fit is not forced to zero. While the attachment rates for carbonate ions are similar to those previous reported, the attachment

rate for calcium for both step orientations are 50-60% of the previous fit at just the saturation index of 0.40. Detachment rates can be neglected, consistent with the lack of near-zero step velocities observed at the higher saturation index. The attachment rate for a calcium ion is similar for both step orientations, however the attachment rate for a carbonate ion is an order of magnitude slower for the acute step than the obtuse step (this was also observed in Stack and Grantham, 2010). Using a heteroscedastic two-tailed *t*-test, the difference between the rates of attachment for a calcium ion were not determined to be statistically significant (*p*-value of 0.4), but the difference between the rates of attachment for a carbonate ion are extremely statistically significant (*p*-value of 0.0008). Since the attachment rate constants for a calcium ion are the same within error and the observed difference in the mean is not statistically different, we assume the attachment rate constants for a calcium ion to either step orientation are the same. Interestingly, it is seemingly the attachment of carbonate ions that is determining the differing calcium-to-carbonate ratio of the peak velocity and the differences in the magnitude of the peak velocity of the growth rate of each of the acute and obtuse steps. These will in turn manifest themselves in the morphologies of the crystals crystal grown under varying calcium-to-carbonate ratio (discussed below).

These differences in kink sites likely leads to the observed asymmetry of step velocities of the different step orientations with respect to ratio, which may indicate the reactions controlling calcite growth for the different step orientations may also be asymmetric (Stack and Grantham, 2010; Perdikouri et al., 2009). Based on varying dependence of the steps on background electrolyte composition, Ruiz-Agudo and coworkers (2011) suggest different processes for the two orientations may control step

velocity. Obtuse step velocity may be controlled by the availability of calcium ions in solution, while acute step velocity may be limited by kink site nucleation and the hydration of the carbonate surface (Ruiz-Agudo et al., 2011). This appears consistent with our observations, at higher supersaturation, obtuse steps advance faster than at lower supersaturation, particularly at high calcium-to-carbonate ratios. For instance, at a ratio of approximately 40, the average step velocity at SI = 0.75 was approximately double the step velocity observed at SI = 0.40, but at a ratio of 0.1, the step velocities were virtually identical at each saturation index. However, the acute steps advance at similar rates at both saturation indices, within error, despite a fifty percent increase in the amount of calcium ions in solution at SI = 0.75 versus SI = 0.40.

3.2 Observations in the presence of strontium.

Step velocities of both step orientations were measured at variable strontium concentrations for five different calcium-to-carbonate ratios (Figure 3.4), three of which were at SI = 0.40 ($[Ca]/[CO_3]$ = 0.111, 2.72, and 12.1) and two of which were at SI =0.75 ($[Ca]/[CO_3]$ = 0.0143 and 27.2). Step velocities were fit using sigmoid curves to provide a quantitative measure of the amount of strontium necessary to inhibit growth and to ease visualization. The choice of functional form is justified below. This functional form is not completely ideal, however, since step velocities of the acute step orientation were sometimes observed to increase slightly at low strontium concentrations, consistent with previous observations (Wasylenki et al., 2005a). Also as in Wasylenki et al. (2005a), as strontium concentration is increased, step advancement rate remained relatively constant until a critical strontium concentration was reached where growth rate collapsed and became almost completely inhibited. However, we find that the amount of

strontium necessary to inhibit growth can vary by more than an order of magnitude under the same saturation index but differing aqueous calcium-to-carbonate ratios (Figure 3.4). At low calcium-to-carbonate ratios, relatively low concentrations of strontium are necessary to inhibit growth, however as the calcium-to-carbonate ratio is increased, progressively higher concentrations of strontium are necessary to produce similar fractions of growth inhibition.

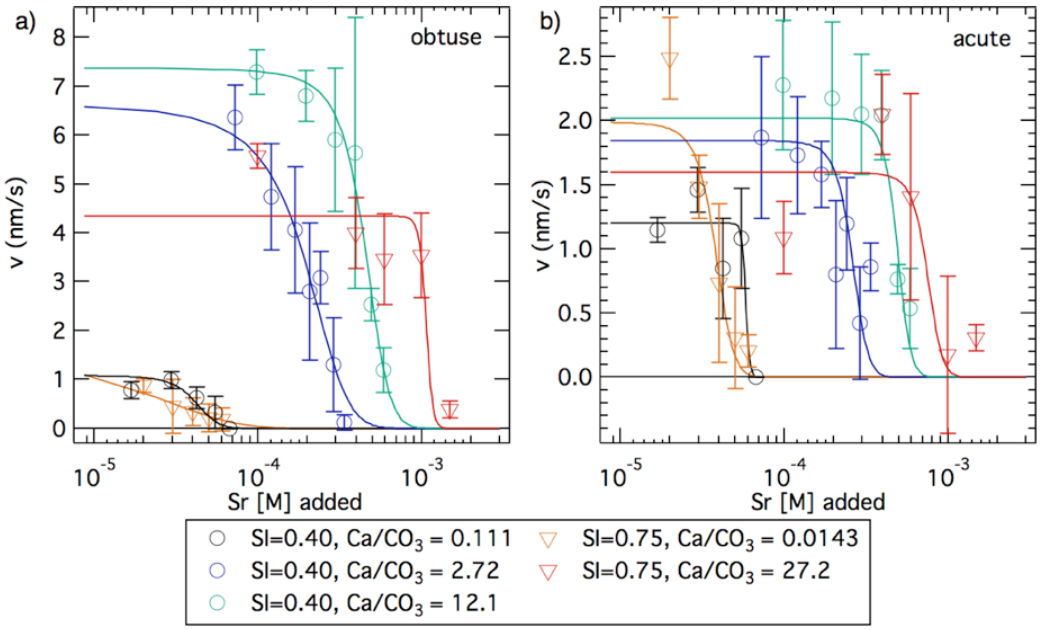

Figure 3.4: Step velocities as a function of the aqueous strontium concentration at a saturation index of 0.40 (circles) and 0.75 (triangles) for the a) obtuse and b) acute step orientations at five different calcium-to-carbonate ratios. We observe significantly higher concentrations of strontium are required to inhibit growth at high calcium-to-carbonate ratios (green circles and red triangles) than near unity (blue circles) or low calcium-to-carbonate ratios (black circles and orange triangles). Error bars are ± 1 standard deviation.

Changes in step velocity were accompanied by morphological changes. In Wasylenki et al. (2005a), rounding and elongation of the steps was observed perpendicular to the *c*-glide plane. While we also observed elongation perpendicular to the *c*-glide plane at all calcium-to-carbonate ratios, the degree of rounding was found to be strongly dependent on ratio. Under solutions with low calcium-to-carbonate ratios ($[Ca]/[CO_3] = 0.0143$) and high strontium concentrations, substantial rounding and bunching of the obtuse steps was observed (Figure 3.5).

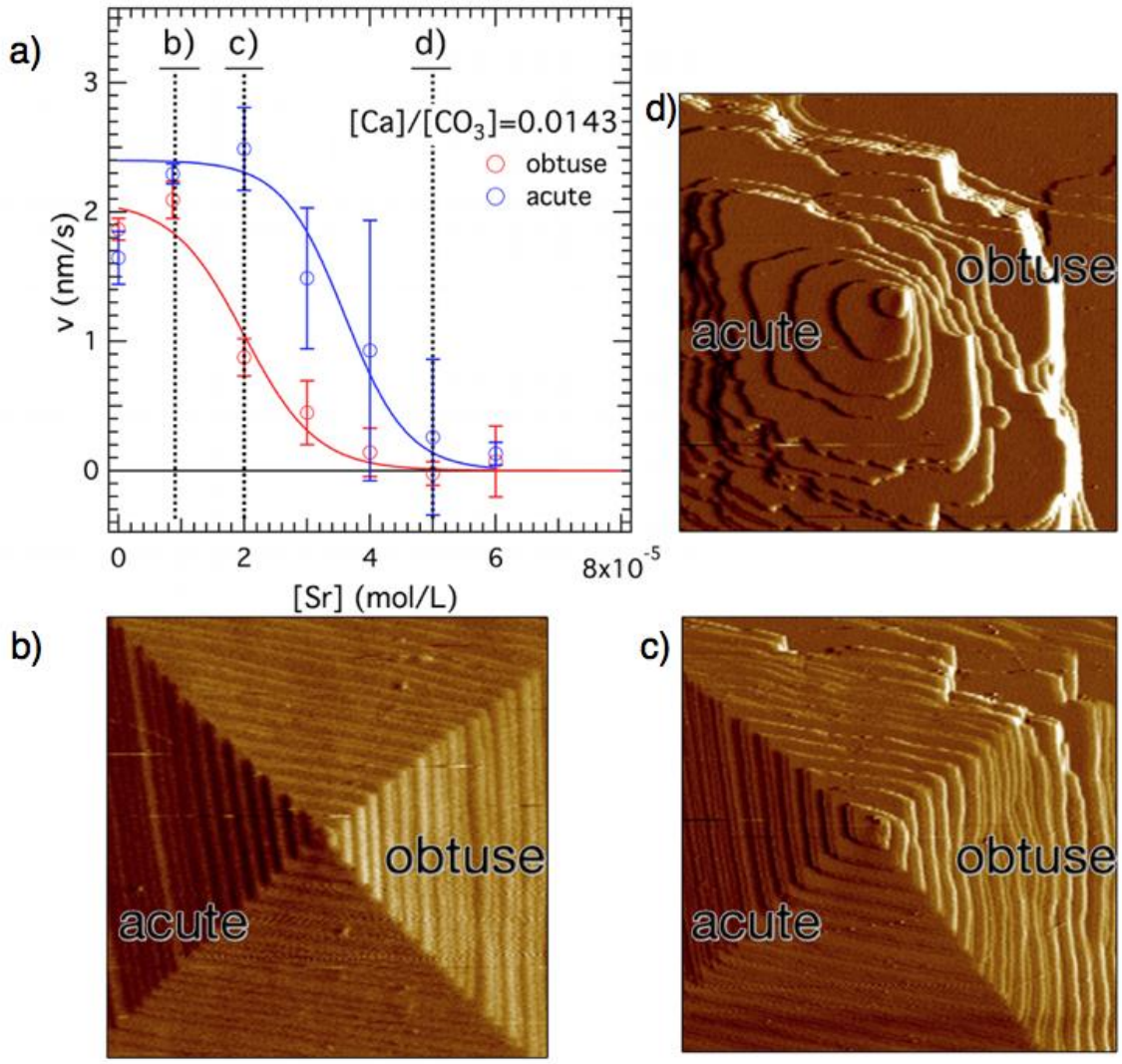

Figure 3.5: Calcite growth morphology at low calcium-to-carbonate ratio ([Ca]/[CO_3] = 0.0143) as a function of the aqueous strontium concentration. Obtuse and acute step orientations are as marked and AFM deflection images correspond to the concentration denoted by the dashed line in a). b) When [Sr] = 8.65×10^{-6} M, acute and obtuse steps advance at similar rates. c) When [Sr] = 2.00×10^{-5} M, step advancement has slowed for the obtuse orientation and obtuse steps begin to round. d) When [Sr] = 5.00×10^{-5} M, obtuse steps become extremely rounded and bunched and steps elongate perpendicular to the c-glide plane. The scan size in b) and c) is 5 μM and 7.5 μM in d).

Significantly less rounding occurred for a given strontium concentration at high calcium-to-carbonate ratios ([Ca]/[CO_3] = 381) (Figure 3.6) and step bunching was exclusive to the acute step orientation (that is, the opposite in the case of the low calcium-to-carbonate ratios). Observations in the absence of strontium were similar to previous

work (Stack and Grantham, 2010): at calcium-to-carbonate ratios greater than 381, bunching of the acute side was observed and at calcium-to-carbonate ratios less than 0.0143, rounding of the obtuse side occurred.

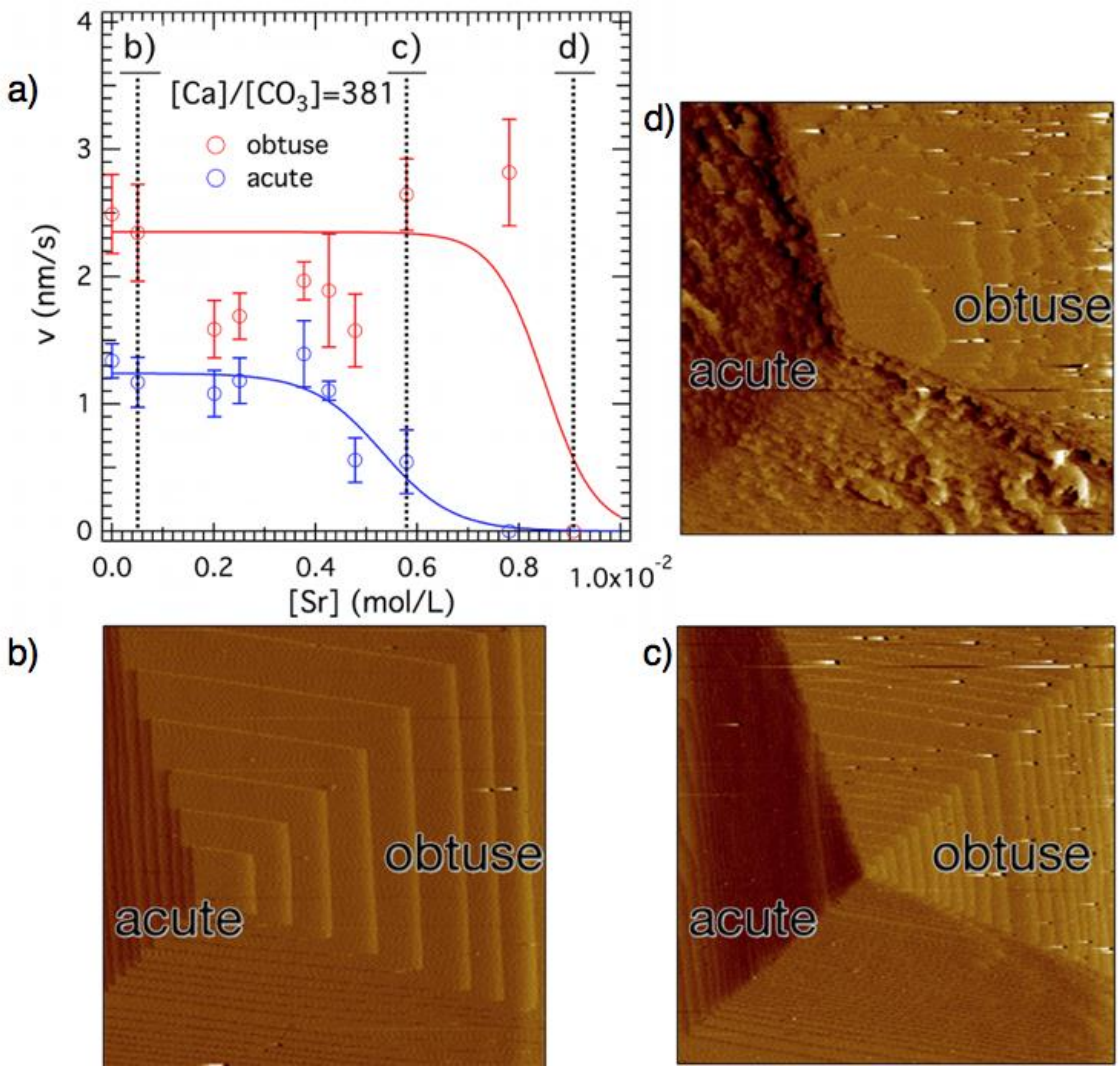

Figure 3.6: Calcite growth morphology at high calcium-to-carbonate ratio ([Ca]/[CO_3] = 381) as a function of the aqueous strontium concentration. Obtuse and acute step orientations are as marked and AFM images correspond to the concentration denoted by the dashed line in a). b) When [Sr] = 5.05×10^{-4} M, acute steps advance slower than obtuse steps. c) When [Sr] = 5.79×10^{-3} M, step advancement of the acute step orientation has slowed. d) When [Sr] = 9.07×10^{-3} M, acute steps have become pinned and rounding of obtuse steps is observed. The scan size in b) is 7.5 μM and 10 μM in c) and d).

It is important to note that the strontium concentration required to inhibit growth increased with both saturation index and calcium-to-carbonate ratio. As saturation index increases, the concentrations of both calcium and carbonate increase, whereas as calcium-to-carbonate ratio increases, the concentration of calcium increases but the concentration of carbonate decreases. This suggests that the concentration of strontium required to inhibit step advancement may correlate with the concentration of aqueous calcium, but not the concentration of aqueous carbonate. To test this hypothesis, we transformed the data in Figure 3.4 to express step velocity as a function of aqueous *strontium-to-calcium* ratio (Figure 3.7).

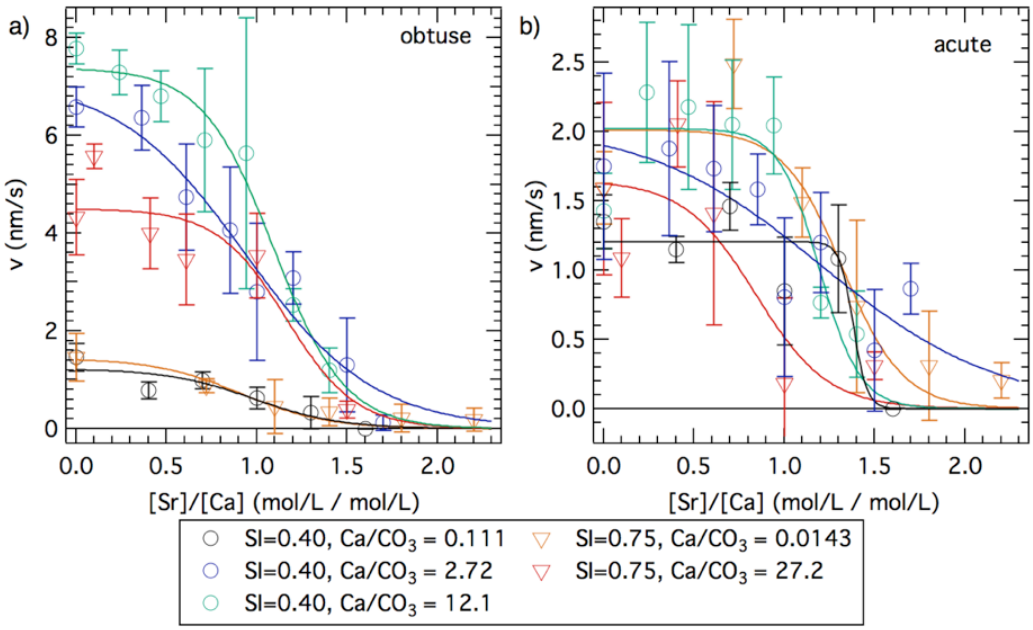

Figure 3.7: Step velocities as a function of the <u>strontium-to-calcium</u> ratio at a saturation index of 0.40 (circles) and 0.75 (triangles) for the a) obtuse and b) acute step orientations at five different calcium-to-carbonate ratios. We observe that growth is usually inhibited at a high strontium-to-calcium ratio, regardless of the calcium-to-carbonate ratio. Error bars are ± 1 standard deviation.

Distinct trends for the obtuse and acute step velocity as a function of the strontium-to-calcium ratio are readily observed. At high strontium-to-calcium ratios, growth is mostly inhibited for both step orientations, even under calcium-to-carbonate ratios where either is limiting. To confirm that there is no correlation between the amount of strontium necessary to inhibit growth and the aqueous carbonate concentration, the step velocities were evaluated as a function of the strontium-to-carbonate ratio (Figure 3.8) and the product of the strontium and carbonate concentrations (Figure 3.9). Our initial hypothesis was that strontium inhibited growth by labializing carbonate ions that adsorbed adjacent to it on the step edge, or by inhibiting their attachment. However, if this mechanism were correct, there would be a dependence of step velocities on either the strontium-to-carbonate ratio or the product of strontium and carbonate. Since a correlation only exists between strontium and calcium and no correlation exists between strontium and carbonate, this mechanism cannot be possible.

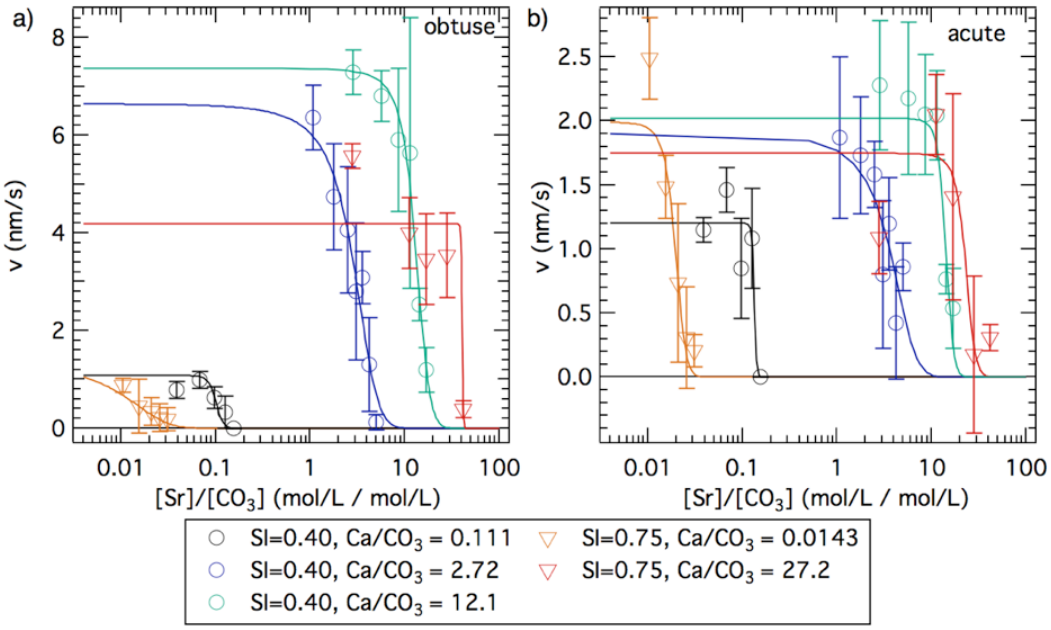

Figure 3.8: Step velocities as a function of the <u>strontium-to-carbonate ratio</u> at a saturation index of 0.40 (circles) and 0.75 (triangles) for the a) obtuse and b) acute step orientations at five different calcium-to-carbonate ratios. We do not observe any correlation between the strontium-to-carbonate ratio and inhibition of growth.

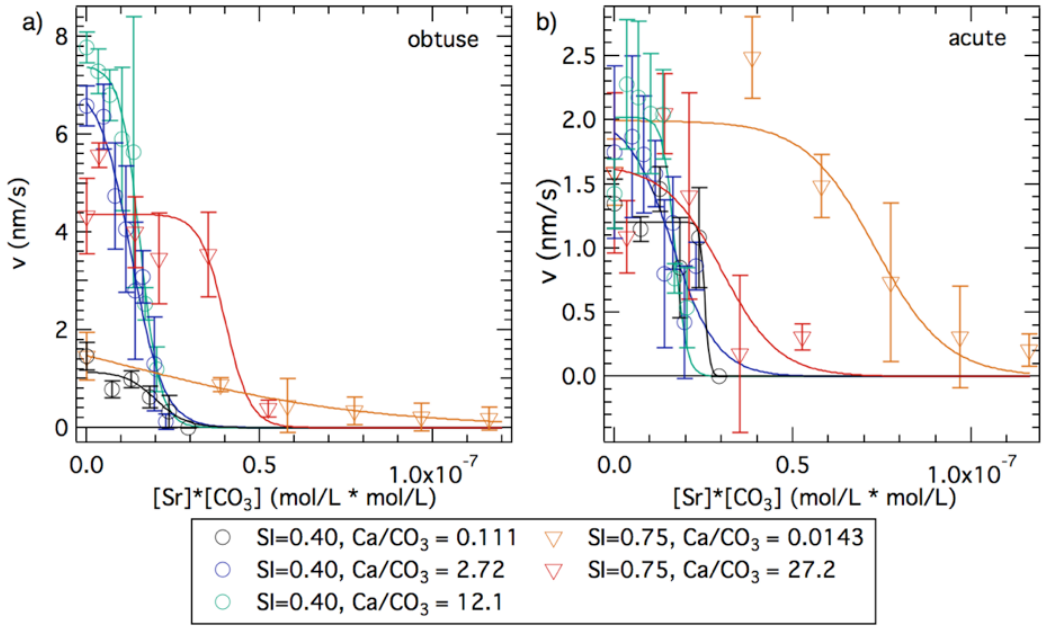

Figure 3.9: Step velocities as a function of the <u>product of strontium and carbonate</u> at a saturation index of 0.40 (circles) and 0.75 (triangles) for the a) obtuse and b) acute step orientations at five different calcium-to-carbonate ratios. We do not observe any correlation between the product of strontium and carbonate and inhibition of growth.

To derive an alternate hypothesis where strontium can only inhibit attachment of calcium, we turn to recent rare event theory simulations for barium detachment/attachment from a barite {120} step edge (Stack et al., 2012). It was found that barium attachment to the step-edge passes through multiple intermediate states prior to becoming a kink site. These include outer-sphere and inner-sphere adsorbed species and a species with two bonds to the surface. If calcium attachment during calcite growth occurs via a similar mechanism, strontium could compete with one or more of these precursor adsorption sites and limit or block attachment of calcium ions to the step edge. For example, simultaneous inner-, outer- and extended outer-sphere adsorption of strontium has been shown to occur on mica surfaces (Lee et al., 2010).

If this conceptual picture is accurate, the choice of a sigmoidal curve would have been prescient, since this allows us to calculate the relative affinity of strontium and calcium sorption to the precursor sites (also sigmoidal curves are appropriate to model equilibrium speciation). If we assume that the step velocity in excess strontium is zero, and the step velocity in the absence of strontium or limited strontium is v_{max}, the sigmoidal curves in Figure 3.7 can be defined as:

$$v = \frac{v_{\max}}{1 + \exp\left(\frac{[\mathrm{Sr}]/[\mathrm{Ca}]_{v_{1/2}} - [\mathrm{Sr}]/[\mathrm{Ca}]}{\alpha}\right)} \tag{3.3}$$

where $[\mathrm{Sr}]/[\mathrm{Ca}]_{v_{1/2}}$ is the strontium-to-calcium ratio at which $v = v_{max}/2$, and α is a parameter which affects the steepness of the curve. For a given strontium-to-calcium ratio and saturation index, the step velocity at which the velocity is one half the maximum velocity indicates the aqueous strontium-to-calcium ratio where the concentrations of

strontium and calcium adsorbed into a precursor state on the step-edge are equal. This may be written as:

$$\text{step}-\text{Sr} \;+\; \text{Ca}_{aq}^{2+} \;\rightleftharpoons\; \text{step}-\text{Ca} \;+\; \text{Sr}_{aq}^{2+} \tag{3.4}$$

where *step-Sr* and *step-Ca* correspond to strontium or calcium adsorbed in a precursor site as described above. Ignoring differences in activity and concentration and solving for the cation exchange constant yields:

$$K_{ex} = \frac{[\text{step}-\text{Ca}][\text{Sr}]}{[\text{step}-\text{Sr}][\text{Ca}]} \tag{3.5}$$

so that where we observe $v = v_{max}/2$, [step-Ca] equals [step-Sr] and the [Sr]/[Ca] ratio is equal to the K_{ex}. The curves in Figure 3.6 yield a mean strontium-to-calcium ratio of 1.09 ± 0.09 for K_{ex} of the obtuse the step orientation (Figure 3.7a) and 1.44 ± 0.19 for the acute step orientation (Figure 3.7b). The close agreement (especially on the obtuse step orientation) indicates that the amount of strontium necessary to inhibit growth correlates with the calcium concentration and supports the concept that strontium acts via competitive inhibition with calcium for some site(s) at the step edge.

To begin to incorporate the effect of strontium into the analytical expressions of step velocity used above, we must first concede that unfortunately step velocities alone cannot provide a unique analytical solution that reflects both the reality of multiple surface structures potentially important (i.e. kink site nucleation and propagation; De Yoreo et al., 2009) and the possibility of multiple precursor adsorption states (i.e., outer-sphere, inner-sphere, etc.; Stack et al., 2012). We modify the rate of kink site nucleation (equation 1.13) to include a possible precursor site by introducing a two-step reaction process:

$$\text{step} + \text{Ca}^{2+}_{aq} \overset{K_{S-Ca}}{\rightleftharpoons} \text{step-Ca} \underset{k_{-2Ca}}{\overset{k_{2Ca}}{\rightleftharpoons}} \text{kink} \tag{3.6}$$

where *step* is the empty precursor site, *step-Ca* is the precursor site with calcium adsorbed, and $K_{S\text{-}Ca}$ is the equilibrium constant for formation of a calcium precursor site. Incorporation of strontium into calcite has been found to be low (~1-2%; Wasylenki et al., 2005a), so here we assume that while strontium adsorbs to an empty precursor site, the rate at which a kink site is subsequently formed is negligible:

$$\text{step} + \text{Sr}^{2+}_{aq} \overset{K_{S-Sr}}{\rightleftharpoons} \text{step-Sr} \tag{3.7}$$

Here, *step-Sr* is the precursor site with strontium adsorbed and $K_{S\text{-}Sr}$ is the equilibrium constant for formation of a strontium precursor site. The total concentration of precursor sites can then be expressed as:

$$[\text{step}]_{total} = [\text{step}] + [\text{step-Ca}] + [\text{step-Sr}] \tag{3.8}$$

and if we substitute [step-Sr] and [step-Ca] from equations 3.6 and 3.7 into this equation, we can determine the concentration of the empty precursor sites:

$$[\text{step}] = \frac{[\text{step}]_{total}}{1 + K_{S-Ca}[\text{Ca}] + K_{S-Sr}[\text{Sr}]} \tag{3.9}$$

This step concentration is related to the attachment rate constant for calcium solved for in Section 3.1 (Table 3.2, Figure 3.3), which can be written as:

$$k_{Ca\ apparent} = k_{Ca\ intrinsic}[\text{step-Ca}] = k_{Ca\ intrinsic} K_{S-Ca}[\text{step}] \tag{3.10}$$

where the apparent rate of attachment of calcium to a kink site is a combination of the intrinsic rate constant, the overall rate at which calcium adsorbs to a precursor site, and the concentration of precursor sites. By taking the ratio of the apparent rate constants in the presence and absence of strontium, we can derive a correction factor (*c.f.*) that can be introduced into the nucleation expression (equation 1.13):

$$c.f. = \frac{1 + K_{S-Ca}[\mathrm{Ca}]}{1 + K_{S-Ca}[\mathrm{Ca}] + K_{S-Sr}[\mathrm{Sr}]} \tag{3.11}$$

such that $k_{Ca\ apparent}$ (with Sr) = $k_{Ca\ apparent}$ (without Sr) × *c.f*, which leads to the following overall expression for the rate of kink site nucleation:

$$R_{kn} = \frac{(k_{Ca} \times c.f.)[Ca]k_{CO_3}[CO_3]}{(k_{Ca} \times c.f.)[Ca] + k_{CO_3}[CO_3]} - k_{-kn} \tag{3.12}$$

To fit this, we used the previously determined attachment rate constants for calcium and carbonate (Table 3.2) in the absence of strontium as fixed parameters and solved for $K_{S\text{-}Ca}$ and $K_{S\text{-}Sr}$ with a Newton-Raphson. The Newton-Raphson minimization was carried out over all the step velocities measured in the presence of strontium and the equilibrium constants can be found in Table 3.3. The resultant fits are shown in Figure 3.10 (obtuse steps, χ^2 = 1609) and Figure 3.11 (acute steps, χ^2 = 358). In particular, it should be stressed that the fit was carried out across all strontium concentrations, aqueous calcium-to-carbonate ratios and saturation indices and that inconsistencies in the zero strontium model will propagate to the data with strontium.

Table 3.3: Estimates of rate constants for the modified nucleation model.

Constants	acute	obtuse
k_{Ca} (s^{-1})	6.4 (± 0.5) × 10^6	6.7 (± 0.3) × 10^6
k_{CO_3} (s^{-1})	4.7 (± 0.4) × 10^6	3.6 (± 0.2) × 10^7
k_{-kn} ($M \cdot s^{-1}$)	0.0 (± 0.02)	0.0 (± 0.02)
$K_{S\text{-}Sr}$	2.9 (± 0.6) × 10^4	1.8 (± 0.3) × 10^4
$K_{S\text{-}Ca}$	1.1 (± 1.2) × 10^3	0.0 (± 2.2) × 10^2

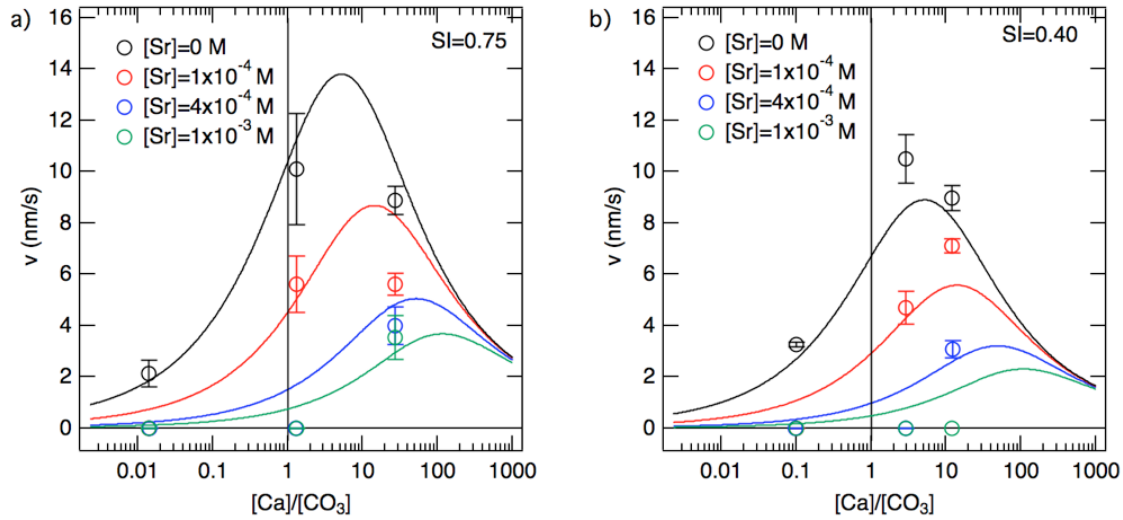

Figure 3.10: Obtuse step velocities as a function of calcium-to-carbonate ratio at a saturation index of a) 0.75 and b) 0.40 at constant strontium concentrations of 0 M (black), 1 × 10^{-4} M (red), 4 × 10^{-4} M (blue), and 1 × 10^{-3} M (green). Curves are model fits of the combined data set (SI = 0.40 and 0.75) using the modified kink site nucleation model (equations 3.11-3.12). Data and model fits in the absence of strontium are the same as in Figure 3.1, but for clarity, only those data points whose calcium-to-carbonate ratio match the strontium experiments are shown.

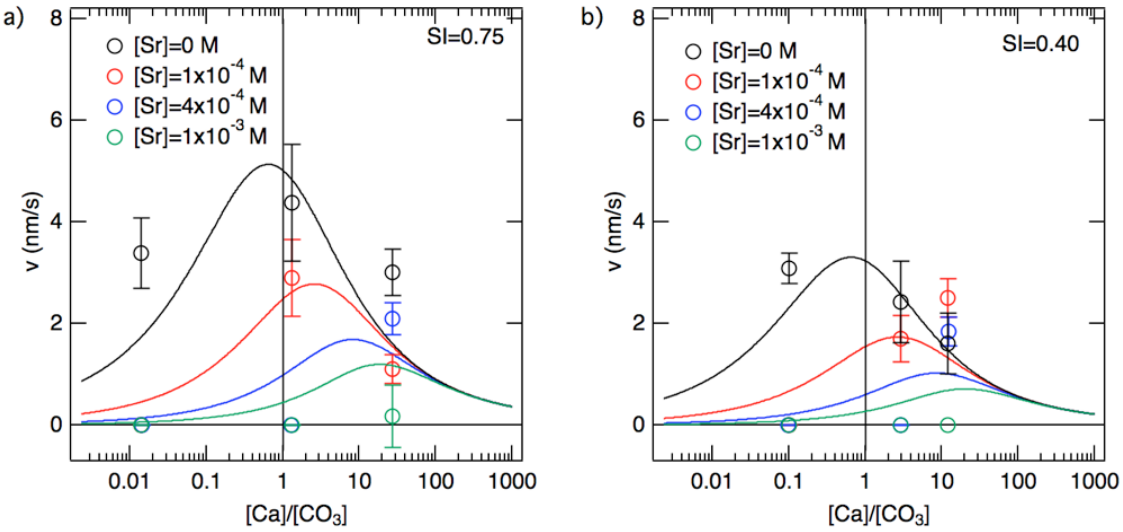

Figure 3.11: Acute step velocities as a function of calcium-to-carbonate ratio at a saturation index of a) 0.75 and b) 0.40 at constant strontium concentrations of 0 M (black), 1 × 10^{-4} M (red), 4 × 10^{-4} M (blue), and 1 × 10^{-3} M (green).

Overall the quality of the fit is quite good, especially for the obtuse step orientation. The fit replicates the overall trend of step velocities decreasing most rapidly at low calcium-to-carbonate concentrations and also predicts the shifting of peak step velocity to higher calcium-to-carbonate ratios with increasing strontium concentrations. The fit also qualitatively captures the trend of non-zero step velocities only being observed under high calcium-to-carbonate ratios. However the fit is unable to replicate the rapidity of which growth becomes inhibited at low calcium-to-carbonate ratios. This may be because we are assuming the propagation of kink sites is much slower than the nucleation of these sites, however the propagation reactions may become more important in these conditions. Other possible sources of error may be improperly describing the back reaction as linear, or assuming that the concentration of precursor sites stays constant throughout our experiments. This likely leads to a propagation of errors that is large enough to lead to the quotient of $K_{S\text{-}Sr}$ and $K_{S\text{-}Ca}$ derived from this analytical expression not being equal to K_{ex} (equation 3.4). The quotient of $K_{S\text{-}Ca}$ and $K_{S\text{-}Sr}$ can be forced to the K_{ex} from the sigmoid fit, but the fit quality is significantly degraded (χ^2 = 3772 and 430 for the obtuse and acute steps, respectively). Overall, we view this model is as good as it reasonably can be without independent confirmation of the reactions that actually occur at the step edges and their rates.

CHAPTER 4: CONCLUSIONS

4.1 Conclusions

Growth rates of calcite were calculated at various calcium-to-carbonate ratios under varying strontium concentration to determine the mechanism by which strontium inhibits calcite growth at two different saturation indices. Step velocities measured in the absence of strontium were modeled using two different crystal growth models. The kinetic ionic ratio model (Zhang and Nancollas, 1998) was unable to replicate experimental step velocities, but the kink site nucleation model (Stack and Grantham, 2010) was able to reproduce the experimental results with fairly good accuracy. Step velocities were also measured in the presence of strontium. At higher saturation indices and higher calcium-to-carbonate ratios, higher concentrations of strontium were required to inhibit calcite growth. This concentration of strontium was found to be correlated with the aqueous strontium-to-calcium ratio, but not with the ratio of strontium-to-carbonate or the product of strontium and carbonate. This implies strontium inhibits attachment of calcium to the calcite surface. Morphology changes were also observed under high strontium concentrations and appeared to be dependent on the aqueous calcium-to-carbonate ratio. At low calcium-to-carbonate ratios, significant rounding of both step orientations was observed and the obtuse step orientation became pinned before the acute step orientation. At high calcium-to-carbonate ratios, the reverse was observed (i.e. the acute step orientation became pinned before the obtuse step orientation) and less rounding was observed. The kink site nucleation model was adapted to account for the

effects of strontium on calcite growth rates, which qualitatively replicates the measured step velocities reasonably well.

4.2 Future Work

The experiments in this study were conducted by increasing the concentration of strontium in solution because we were unsure of what concentration of strontium would be required to inhibit growth for each of the different calcium-to-carbonate ratios. However, now that we know the approximate concentrations required, it may be useful to perform some similar experiments at constant strontium concentration and vary the calcium-to-carbonate ratio rather than the strontium concentration. These experiments would need to be carried out at low strontium concentration (1×10^{-4} M or lower) because at higher strontium concentrations step velocities decrease at a stoichiometric aqueous calcium-to-carbonate ratio. It would be important to choose a strontium concentration that does not affect the measured step velocities at a ratio of unity because varying calcium-to-carbonate ratio experiments are started at stoichiometric calcium-to-carbonate ratios and then the solution composition is either varied with increasing calcium-to-carbonate ratio or decreasing calcium-to-carbonate ratio. Starting experiments at ratios an order of magnitude higher or lower than unity consistently leads to lower step velocities than those measured otherwise, indicating changing the calcium-to-carbonate ratio irreversibly affects calcite growth.

Additionally, as step velocities are not be able to solely provide the information necessary to develop a crystal growth theory which can accurately reproduce experimental results, use of metadynamics or other independent information about the reactions occurring on a step will be necessary to calculate the effect strontium has on the

apparent rate of attachment calcium, as well as examine possible ways strontium is blocking attachment.

The applicability of the modified kink site nucleation model (equations 3.12) could be tested by performing similar experiments in the presence of magnesium (Wasylenki et al., 2005b) or silicic acid (Pina et al., 2009), which have also been found to decrease calcite growth rates. While these both affect calcite growth rates, the morphology changes observed differ from those observed in the presence of strontium. While strontium causes elongation of growth hillocks perpendicular to the c-glide plane, magnesium and silicic acid cause elongation of calcite growth hillocks parallel to the c-glide plane. This is likely because magnesium, and possibly silicic acid, preferentially affect the acute step orientation, while strontium preferentially affects the obtuse step direction due to the different sizes of the molecules.

REFERENCES

Berner, R. A. *Amer. J. Sci.* **1978**, *278*, 1235.

Burton, W. K.; Cabrera, N.; Frank, F. C. *Phil. Trans. R. Soc.* **1951**, *243*, 299.

Chandler, D. Introduction to Modern Statistical Mechanics. Oxford University Press, New York, **1987**.

Cohen, A. L.; McConnaughey, T.A. *Rev. Min. Geochem.* **2003**, *54*. 151.

de Villiers, S.; Shen, G. T.; Nelson, B. K. *Geochim. Cosmochim. Acta* **1994**, *58*, 197.

De Yoreo, J. J.; Zepeda-Ruiz, L. A.; Friddle, R. W.; Qiu, S. R.; Wasylenki, L.E.; Chernov, A. A.; Gilmer, G. H.; Dove, P. M. *Cryst. Growth Des.* **2009**, *9*, 5135.

De Yoreo, J. J.; Vekilov, P. G. *Rev. Mineral. Geochem.* **2003**, *54*, 57.

DePaolo, D.J. *Geochim. Cosmochim. Acta* **2011**, *75*, 1039.

Duenas-Bohorquez, A.; Raitzsch, M.; de Nooijer, L. J..; Reichart, G. J. *Marine Micropalentology* **2011**, *81*, 122.

Fan, C. F.; Chen, J.; Chen, Y.; Ji, J. F.; Teng, H. H. *Geochim. Cosmochim. Acta* **2006**, *70*, 3820.

Frenkel, J. *J Phys USSR* **1945**, *9*, 392.

Gratz, A. J.; Hillner, P. E.; Hansma, P. K. *Geochim. Cosmochim. Acta* **1993**, *57*, 491.

Gebrehiwet, T. A.; Redden, G. D.; Fujita, Y.; Beig, M. S.; Smith, R. W. *Geochem. Trans.* **2012**, *13*, 1.

Kerisit, S.; Parker, S. C. *J. Am. Chem. Soc.* **2004**, *126*, 10152.

Kossel, W *Nachr. Ges. Wiss.* Gottingen **1927**, 135.

Kowacz, M.; Putnis, C. V.; Putnis, A. Geo*chim. Cosmochim. Acta* **2007**, *71*, 5168.

Land, T. A.; De Yoreo, J. J; Lee, J. D. *Surf. Sci.* **1997**, *384*, 136.

Larsen, K.; Bechgaard, K.; Stipp, S.L.S. *Geochim. Cosmochim. Acta* **2010**, *74*, 2099.

Lasaga, A. C. Kinetic Theory in the Earth Sciences. Princeton University Press, New Jersey, **1998**.

Lea, D. W.; Mashiotta, T. A.; Spero, H. J. *Geochim. Cosmochim. Acta* **1999**, *63*, 2369.

Lee, S. S.; Fenter, P.; Park, C.; Sturchio, N. C.; Nagy, K. L. *Langmuir* **2010**, *26*, 16647.

Lorens, R. B. Geo*chim. Cosmochim. Acta* **1981**, *45*, 553.

Parkhurst, D. L. *User's Guide to PHREEQC: A Computer Program for Speciation, Reaction-Path, Advective-Transport, and Inverse Geochemical Calculations.* U.S. Geological Survey Water-Resources Investigations Report 95, 1995.

Perdikouri, C.; Putnis, C. V.; Kasioptas, A.; Putnis, A. *Cryst. Growth Des.* **2009**, *9*, 4344.

Pina, C. M.; Merkel, C.; Guntram, J. *Cryst. Growth Des.* **2009**, 9, 4084.

Pingitore, N. E.; Lytle, F. W.; Davies, B. M.; Eastman, M. P.; Eller, P. G.; Larson, E. M. *Geochim. Cosmochim. Acta* **1992**, *56*, 1531.

Plummer, L. N.; Busenberg, E. *Geochim. Cosmochim. Acta* **1982**, *46*, 1011.

Raitzsch, M.; Duenas-Bohorquez, A.; Reichart, G. J.; De Nooijer, L. J.; Bickert, T. *Biogeosciences* **2010**, *7*, 869.

Rashkovich, L. N.; De Yoreo, J. J.; Orme, C. A.; Chernov, A. A. *Crystogr. Rep.* **2006**, *51*, 1063.

Reeder, R. J. *Rev. Mineral. Geochem.* **1983**, *11*, 1.

Richens, D. T. *The Chemistry of Aqua Ions*. Wiley and Sons, New York (1997).

Riley, R. G.; Zachara, J. M.; Wobber, F. J. DOE/ER-0547T. US Department of Energy, Office of Energy Research: Washington, DC, 1992, 1.

Ruiz-Agudo, E.; Putnis, C. V.; Wang, L.; Putnis, A. *Geochim. Cosmochim. Acta* **2011**, *75*, 3803.

Russell, A. D.; Honisch, B.; Spero, H. J.; Lea, D. W. *Geochim. Cosmochim. Acta* **2004**, *68*, 4347.

Sayani, H. R.; Cobb, K. M.; Cohen, A. L.; Elliott, W. C.; Nurhati, I. S.; Dunbar, R. B.; Rose, K. A.; Zaunbrecher, L. K. *Geochim. Cosmochim. Acta* **2011**, *75*, 6361.

Speer, J. A. *Rev. Mineral. Geochem.* **1983**, *11*, 145.

Stack, A. G. *J. Phys. Chem. C* **2009**, *113*, 2104.

Stack, A. G.; Grantham, M. C. *Cryst. Growth Des.* **2010**, *10*, 1409.

Stack, A. G.; Raiteri, P.; Gale, J. D. *J. Am. Chem. Soc.* **2012**, 134, 11.

Stranski, I. N. *Z. Phys. Chem.* **1928**, *136*, 259.

Tai, C. Y.; Lu, J. H.; Wu, J. K. *J. Chin. Inst. Chem. Eng.* **2005**, *36*, 443.

Tang, J. W.; Koehler, S. J.; Dietzel, M. *Geochim. Cosmochim. Acta* **2008**, *72*, 3718.

Tartakovsky, A. M.; Redden, G.; Lichtner, P. C.; Schiebe, T. D.; Meakin, P. *Wat. Resour. Res.* **2008**, *44*, W06S04.

Teng, H. H.; Dove, P. M.; De Yoreo, J. J. *Geochim. Cosmochim. Acta* **2000**, *64*, 2255.

Tesoriero, A. J.; Pankow, J. F. *Geochim. Cosmochim. Acta* **1996**, *60*, 1053.

Thomas, T. N.; Land, T. A.; Martin, T.; Casey, W. H.; De Yoreo, J. J. *J. Cryst. Growth* **2004**, *260*, 566.

Vere, A. W. Crystal Growth: Principles and progress. Plenum Press, New York, **1987**.

Wasylenki, L. E.; Dove, P. M.; Wilson, D. S.; De Yoreo, J. J. *Geochim. Cosmochim. Acta* **2005a**, *69*, 3017.

Wasylenki, L. E.; Dove, P. M.; De Yoreo, J. J. *Geochim. Cosmochim. Acta* **2005b**, *69*, 4227.

Zhang, J. W.; Nancollas, G. H. *J. Coll. Int. Sci.* **1998**, *200*, 131.